March 2006

Nanomagnetic Models

Ralph Skomski
University of Nebraska-Lincoln, rskomski2@unl.edu

Jian Zhou
University of Nebraska - Lincoln

Published (as Chapter 3) in *Advanced Magnetic Nanostructures*, edited by David Sellmyer and Ralph Skomski, Springer, 2006.

Nanomagnetic Models

Ralph Skomski and Jian Zhou

Center for Materials Research and Analysis and
Department of Physics and Astronomy
University of Nebraska
Lincoln, NE 68588, USA

Abstract – The atomic-scale and mesoscopic physics of magnetic nanostructures is reviewed. Emphasis is on the description of magnetic phenomena and properties by analytical models, as contrasted to numerical approaches. Nanostructuring affects the magnetic properties on different length scales, from a few interatomic distances for intrinsic properties such as magnetization and anisotropy to more than 10 nm for extrinsic properties, such as coercivity. The consideration includes static and dynamic mechanisms, as well as nanoscale finite-temperature effects. Some explicitly discussed examples are Curie-temperature changes due to nanostructuring, the effect of narrow and constricted walls, the potential use of magnetic nanodots for finite-temperature quantum computing, and exchange-coupled hard-soft nanocomposites. The temperature dependence of extrinsic properties reflects the atomic-scale static or 'intrinsic' temperature dependence of the free-energy barriers and thermally activated dynamic or 'extrinsic' jumps over metastable free-energy barriers.

I. INTRODUCTION

Nanomagnetism involves both atomic and macroscopic features, but it cannot be reduced to a superposition of these two limits. Macroscopic interactions, as exemplified by the compass needle and the geomagnetic field, and atomic-scale magnetic phenomena, such as quantum-mechanical exchange [1–4], are necessary but not sufficient to understand nanomagnetism. Solid-state matter is made from atoms, and the corresponding length scale, Bohr's radius a_o = 0.52 Å, determines the range of the exchange responsible for bonding and magnetism. On the other hand, Maxwell's equations are macroscopic, that is, they do not correspond to any characteristic length. Why are the phenome-

na considered in this book realized on a length scale of a few nanometers, as contrasted to, for example, a few meters?

An answer is provided by the relativistic nature of many magnetic phenomena of importance in nanomagnetism [5, 6]. For example, typical domain walls have a thickness of few nanometers. This length reflects the competition between nonrelativistic exchange and relativistic magnetic anisotropy. A simple but qualitatively correct picture is obtained from the relativistic electron energy $mc^2\sqrt{1+v^2/c^2}$, where v is the electron velocity. Expanding the energy into powers of v/c yields the rest energy mc^2, the electrostatic or 'nonrelativistic' energy $mv^2/2$, and the lowest-order relativistic correction $(\alpha/2)^2 mv^2/2$, where $\alpha = 4\pi\varepsilon_0 e^2/\hbar c$ is Sommerfeld's fine-structure constant. Here we have exploited that typical electron velocities in solids are of order $v = \alpha c$. Respective examples of nonrelativistic and relativistic magnetic interactions are exchange, which has the character of an integral over electrostatic interactions, and spin-orbit coupling, which leads to magnetocrystalline anisotropy [7, 8]. On an atomic scale, relativistic interactions are unable to compete against atomic-scale exchange effects. For example, Heisenberg exchange may exceed 1000 K, whereas typical anisotropies are less than 1 K. However, electrostatic and relativistic contribution become comparable on length scales of order $a_0/\alpha = 7.25$ nm [5, 6, 9].

In addition to the range of interactions, there is the question of interference with structural length scales. For example, Bloch wave functions, which form the basis for the band-structure theory of itinerant magnetism, require infinite crystals with perfect periodicity. How does nanostructuring interfere with this requirement? Similarly, from a thermodynamic point of view, ferromagnetism is limited to infinite crystals. It fact, the spontaneous magnetization of any finite magnet is zero, because thermal fluctuations cause the magnetization to average. This leads to the next consideration, the dependence of equilibration or averaging times on structural length scales.

There is a fundamental distinction between intrinsic and extrinsic properties. Examples of *intrinsic* properties are the spontaneous magnetization M_s, the Curie temperature T_c, and the anisotropy K_1. Intrinsic properties describe perfect crystals or surfaces, but their physical origin is atomic and involves quantum phenomena such as exchange, crystal-field interaction, interatomic hopping, and spin-orbit coupling [1, 2, 8, 10, 11]. Intrinsic properties tend to approach their bulk values on fairly small length scales. For example, 'long-range' thermodynamic fluctuations, as involved in the realization of the Curie temperature, and deviations from the Bloch character of metallic wave functions yield only small corrections when the size of the magnetic particle exceeds about 1 nm. The dynamics is characterized by fast equilibration times which means that intrinsic properties can be treated

by equilibrium statistical mechanics. This makes it possible to treat intrinsic properties as local parameters. For example, $M_s(\mathbf{r})$ and $K_1(r)$ reflect the local chemistry, and the unit vector $\mathbf{n}(\mathbf{r})$ of the easy magnetization direction corresponds to the local c-axis orientation of the crystallites.

Extrinsic or hysteretic magnetic properties, such as the coercivity H_c and the remanence M_r, reflect the magnet's real-structure [12–16]. For example, the coercivity of technical iron doubles by adding 0.01 wt.% nitrogen [15]. Such small concentrations have little effect on the intrinsic properties but lead to inhomogeneous lattice strains that affect the propagation of magnetic domain walls and explain the observed coercivity increase. The hysteretic character of extrinsic properties means that equilibration times may be very long. At room temperature, the switching of a single atomic moment is a frequent event, but the thermally activated switching of nanoscale cooperative units, such as domain-wall segments, is very rare. This is the thermodynamic origin of hysteresis, enabling us to build permanent magnets and to store information on magnetic disks.

This chapter investigates how intrinsic and extrinsic properties are affected by nanostructuring. Emphasis is on model calculations and analytical approximations, as contrasted to Chapter 2 by Kashyap *et al.* which focuses on numerical calculations, and Ch. 4 by Schrefl *et al.,* where emphasis is on micromagnetic models and simulations. Section 2 is devoted to static properties, whereas section 3 is concerned with magnetization dynamics. Finally, section 4 presents a number of case studies.

2. MESOSCOPIC MAGNETISM

2.1. Nanoscale Spin Structure

2.1.1. Magnetic moment

The magnetic moment nearly exclusively originates from the spin and orbital moments of transition-metal electrons. The magnetic moment of iron-series transition-metal atoms in metals (Fe, Co, Ni, YCo_5) and nonmetals (Fe_3O_4, NiO) is largely given by the *spin*, and the moment, measured in μ_B, is equal to the number of unpaired spins. The orbital moment is very small, typically of the order of 0.1 μ_B, because the orbital motion of the electrons is quenched by the crystal field [16–18]. By contrast, rare-earth moments are given by Hund's rules, which predict the spin and orbital moment as a function of the number of inner-shell electrons [17]. In some cases, atoms are spin-polarized by neighboring atoms. An example of importance in nanomagnetism is $L1_0$ magnets such as FePt, where the Pt carries a magnetic moment.

The spin moment is largely determined by intra-atomic exchange. It is an electrostatic many-body effect, caused by the $1/|\mathbf{r} - \mathbf{r'}|$ Coulomb interaction between electrons located at **r** and **r'**. Physically, ↓↑ electron pairs in an atomic orbital are not forbidden by the Pauli principle but are unfavorable from the point of view of Coulomb repulsion. Parallel spin alignment, ↑↑, means that the two electrons are in different orbitals, which is electrostatically favorable. However, the corresponding gain in Coulomb energy competes against an increase in one-electron energies, because one of the two electrons must occupy an excited state.

The magnetic moments of insulating transition-metal oxides and rare-earth metals are located on well-defined atomic sites. However, in Fe, Co, and Ni, as well as in many alloys, the moment is delocalized or *itinerant*. Nonmagnetic metals, or Pauli paramagnets, have two equally populated ↑ and ↓ subbands; and an applied magnetic field transfers a few electrons from the ↓ band to the ↑ band. The corresponding spin polarization is very small, of the order of 0.1 %, because the Zeeman interaction is a small relativistic correction [19]. Itinerant ferromagnetism is realized by narrow bands, where the intraatomic exchange is stronger than the band-width related gain in single-electron hybridization (Stoner criterion).

The Bloch character of itinerant wave functions means that the wave functions extend to infinity. This is not realistic for two reasons. First, magnets encountered in reality, in particular nanomagnets, cannot be considered as infinite. Second, finite-temperature excitations create spin disorder and break the Bloch symmetry of the ↑ and ↓ wave functions. The problem of nonequivalent sites can be tackled, for example, by real-space approaches [16, 20–23]. Restricting the consideration to nearest neighbors yields the correct band width, but details of the band structure, such as peaks in the density of states, are ignored. Increasing the number of neighbors improves the resolution of the density of states and makes it possible to distinguish between bulk sites and sites close to surfaces. As a consequence, magnetic moments are determined by the local atomic environment, typically without major nanoscale corrections.

2.1.2. Interatomic exchange

The spin structure of a magnetic moment is the relative orientation of the atomic magnetic moments. It includes types of zero-temperature magnetic order, such as ferromagnetism, ferrimagnetism, and antiferromagnetism, and finite temperature magnetic order. However, micromagnetic structures, such as domains and domain walls, are usually excluded from the consideration. Figure 1 shows some spin structures of interest in the present context.

To a large extent, the spin structure of bulk and nanomagnets is determined by the interatomic Heisenberg exchange, $J(\mathbf{R}_i - \mathbf{R}_j)\,\mathbf{S}_i \cdot \mathbf{S}_j = J_{ij}\,\mathbf{S}_i \cdot \mathbf{S}_j$. For

positive and negative values of J_{ij} it favors parallel and antiparallel spin alignment, respectively. In ferromagnets, such as Fe, Co, and $Nd_2Fe_{14}B$, all spins are parallel and the atomic moments add. Ferrimagnets, such as Fe_3O_4 and $BaFe_{12}O_{19}$, and antiferromagnets, such as CoO and MnF_2, are characterized by two (or more) sublattices with opposite moments. This amounts to a ferrimagnetic reduction or antiferromagnetic absence of a net moment. Sublattice formation may be spontaneous, as in typical antiferromagnets, or imposed by the atomic composition, as in ferrimagnets [24] [25]. In metals, the interatomic exchange may be positive or negative and depends on the atomic environment, on the interatomic distance, and on the band filling.

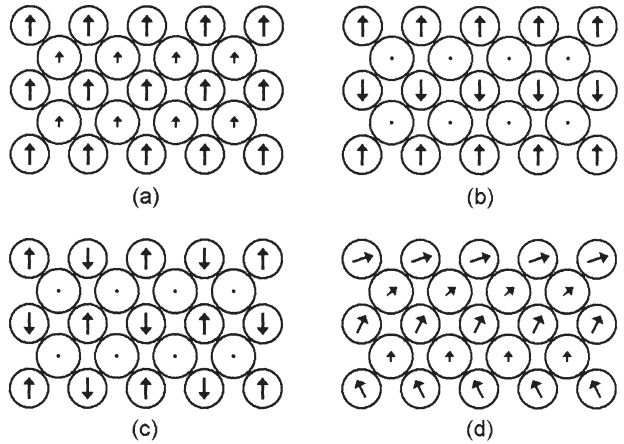

Figure 1. Spin structures (schematic): (a) ferromagnetism, (b–c) antiferromagnetism, and (d) noncollinear structure. The shown structure of the $L1_0$ type; the small atoms (with the large magnetization arrows) the iron-series transition-metal atoms, as compared to the bigger 4d/4f atoms. Examples of $L1_0$ magnets are CoPt and FePt.

A simple and asymptotically correct [26–28] model is the Ruderman-Kittel-Kasuya-Yosida or RKKY exchange between two localized moments in a Pauli-paramagnetic matrix. For a free-electron gas of wave-vector k_F,

$$J_{ij} = J(|\,\mathbf{r}_i - \mathbf{r}_j\,|) = J(R) \sim \cos(2k_F R)/R^3 \qquad (1)$$

The interaction is obtained by second-order perturbation theory, that is, the embedded magnetic moments lead to a mixing of one-electron wave functions. The origin of the oscillations is the sharp Fermi surface, which means

that spatial features smaller than about $1/k_F$ cannot be resolved with available zero-temperature wave functions.

RKKY interactions were first considered on an atomic scale, where the oscillation period is on an Å scale. In nanostructures, the fast oscillations do not average to zero but increase with the size of the embedded clusters or nanoparticles. However, the increase is less pronounced than that of magnetostatic interactions, and for particles sizes larger than about 1 nm, the magnetostatic interactions become dominant [27, 29]. In semiconductors and semimetals, such as Sb, the low density of carriers means that k_F is small, and the period of the oscillations is nanoscale [16, 28]. This contributes to the complexity of the physics of diluted magnetic semiconductors [30, 31].

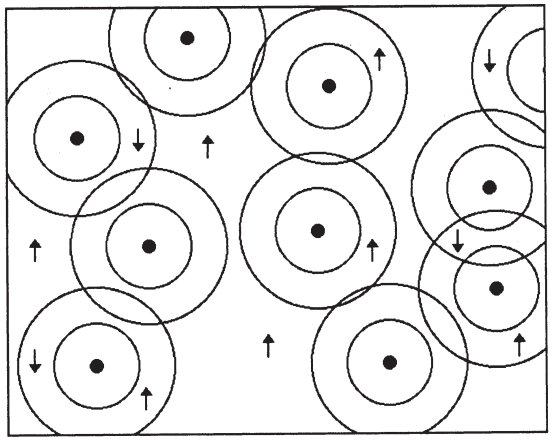

Figure 2. Carrier mediated exchange in dilute semiconductors (schematic). The mechanism is similar to RKKY interactions, but due to the essential involvement of donor or acceptor orbitals, $J(r_i, r_j)$ can no longer be written as $J(|r_i - r_j|)$.

In a strict sense, the RKKY interaction is mediated by free electrons, but there exist similar effects in other regimes, for example in the tight-binding scheme [32]. Figure 2 shows the example of a dilute magnetic semiconductor where localized impurity spins are coupled by shallow donor or acceptor carriers. The carrier orbitals have a radius of the order of 1 nm, hybridize, and yield an RKKY -type coupling. A simple case is the exchange mediated by a two weakly overlapping s-orbitals, centered at $\mathbf{R}_1$ and $\mathbf{R}_2$. The overlap leads to bonding and antibonding orbitals, and the exchange. J_{ij} is obtained from the hybridized electrons by second-order perturbation theory. In terms of local electron densities $\rho(\mathbf{r}) = \psi^*(\mathbf{r})\psi(\mathbf{r})$, the exchange J_{ij} scales as $(\rho(\mathbf{r}_i - \mathbf{R}_1) - \rho(\mathbf{r}_i - \mathbf{R}_2))\,(\rho(\mathbf{r}_j - \mathbf{R}_1) - \rho(\mathbf{r}_j - \mathbf{R}_2))$. This means that the exchange is ferromagnetic if the magnetic ions are located in the same shallow s-orbital and antiferromagnetic if they are in different s-orbitals. Correlations (the Hubbard or 'Coulomb-blockade' energy of the orbitals) can be shown to reduce the ferromagnetic exchange while leaving the qualitative picture unchanged.

One effect of competing RKKY exchange is noncollinear spin structures, as illustrated in Fig. 1(d). Noncollinearity due to competing exchange is encountered, for example, in some elemental rare earths (helimagnetism), where it reflects different exchange interactions between nearest and next-nearest rare-earth layers [33]. Note that the corresponding magnetization wave vector is generally incommensurate with lattice spacing, not only in nanostructures but also in perfect crystals. Furthermore, the effect is relatively strong, with angles between neighboring atomic spins from 0 to 180°. This is in contrast to the relativistic effects considered in the next subsection.

2.1.3. Exchange stiffness

On a continuum level, the Heisenberg exchange energy of a cubic material is

$$E_{ex} = \int A(\nabla(\mathbf{M}/M_s))^2 \, dV \tag{2}$$

where A is the *exchange stiffness.* More generally, Heisenberg exchange is described by

$$E_{ex} = \iint J(\mathbf{r} - \mathbf{r}')\, \mathbf{M}(\mathbf{r})\cdot\mathbf{M}(\mathbf{r}')\, dV dV' \tag{3}$$

A well-known derivation of Eq. (2) is in terms of magnetization angles. It, assumes $\varphi = 0$, so that $E_{ex} = \int A(\nabla\theta)^2 dV$, and takes into account that $\Sigma_{ij} J_{ij} \cos(\theta_i - \theta_j) \approx \Sigma_{ij} J_{ij} (1 - (\theta_i - \theta_j)^2/2)$. Using the expansion $\theta_j = \theta_i + \nabla\theta \cdot (\mathbf{r}_j - \mathbf{r}_i)$ and comparing the result with Eq. (2) then yields $A \sim \Sigma_{ij} J_{ij} (\mathbf{r}_i - \mathbf{r}_j)^2$. This result is meaningful for nearest-neighbor interactions, but it diverges for long-range interactions J_{ij}. An example is the RKKY interaction, where integration over all neighbors yields $A \sim \int 1/R^3 \; R^2 \; R^2 \; dR = \infty$. This is because $\theta_j = \theta_i + \nabla\theta \cdot (\mathbf{r}_j - \mathbf{r}_i)$ breaks down for large distances $R = |\, \mathbf{r}_i - \mathbf{r}_j \,|$.

A more general derivation of A is based on Fourier transformation, which diagonalizes $J(|\mathbf{r} - \mathbf{r}'|)$ and yields a representation in terms of J_k. Since $\int A(\nabla\theta)^2 dV = \int J_k \, \theta_k^2 \, d\mathbf{k}$ and $\int A(\nabla\theta)^2 dV = -\int A \, k^2 \, \theta_k^2 \, d\mathbf{k}$, A is given by the quadratic coefficient of the expansion of J_k with respect to $\mathbf{k}$. Putting $\mathbf{k} = k\mathbf{e}_k$, $\mathbf{R} = R\cos\theta'\mathbf{e}_k + R\sin\theta'\mathbf{e}_\perp$, and $dV = 4\pi R^2 \sin\theta' \, d\theta' \, dR$ yields

$$J_k \sim \int J(R) \frac{\sin(kR)}{kR} R^2 \, dR \tag{4}$$

Here $J_k = F(|\mathbf{k}|)$ is the Lindhard screening function [26, 34]. Note that noncollinear or incommensurate spin states then correspond to a minimum of $J(\mathbf{k})$.

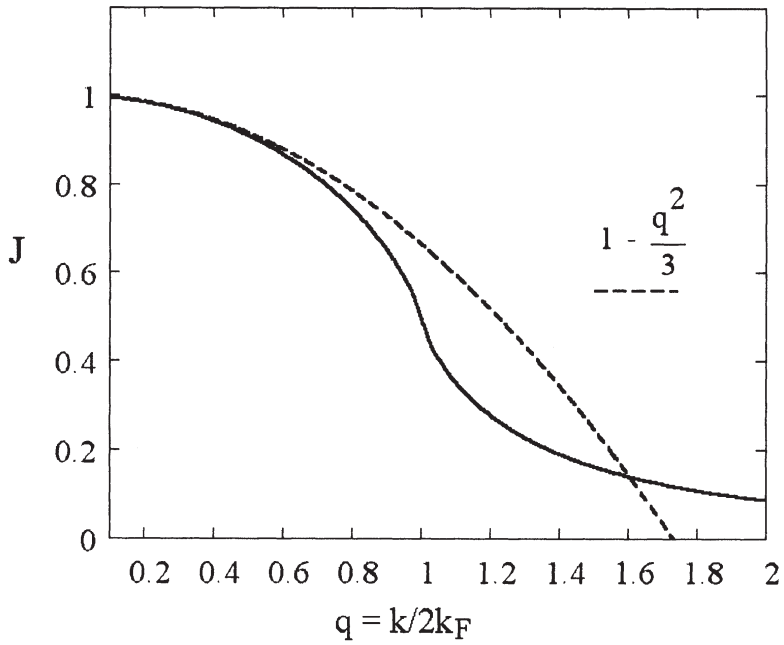

Figure 3. Exchange energy as a function of the wave vector of the magnetization inhomogenity: Lindhard function (solid line) and exchange-stiffness or continuum approximation (dashed line). For late 3d elements (Cu), $k/2k_F = 1$ corresponds to modulation wavelength of 0.23 nm.

Figure 3 compares the Lindhard function (solid line) with the exchange- stiffness approximation (dashed line). We see that the exchange-stiffness approximation works well unless k is comparable to k_F.

In *noncubic materials*, A must be replaced by the 3 × 3 exchange-stiffness tensor $A_{\mu\nu}$, and the energy is $\Sigma_{\mu\nu} \int A_{\mu\nu}\, \partial\mathbf{M}/\partial x_\mu \cdot \partial\mathbf{M}/\partial x_\nu \, dV$. Here the indices μ and ν denote the spatial coordinates x, y, and z of the bonds. The energy is anisotropic with respect to the nabla operator $\nabla_\mu = \partial/\partial_\mu$ (bond anisotropy) but isotropic with respect to the magnetization $\mathbf{M}$. By contrast, the relativistic anisotropic exchange $\Sigma_{\alpha\beta} \int A_{\alpha\beta}\, \nabla M_\alpha\, \nabla M_\beta \, dV$ is isotropic with respect to ∇ but anisotropic with respect to $\mathbf{M}$.

2.1.4. Curie temperature

Thermal disorder competes against interatomic exchange and causes the magnetization of ferromagnets to vanish at a well-defined sharp Curie temperature T_c. In a strict sense, ferromagnetism is limited to infinite magnets, because thermal excitations in finite magnets cause the net moment to fluctuate between opposite directions. The Curie temperature is determined by the site-resolved exchange coefficients. J_{ij}, and since M_s and T_c are equilibrium properties, it is sufficient to know the *partition junction* $Z = \Sigma_\mu \exp(-E_\mu/k_B T)$, where the summation includes all microstates or spin-configurations μ. However, the number of terms in Z increases exponentially with the size of the magnet, and there exist exact solutions only in a few cases [35]. The simplest approximation is the *mean-field approximation*, where the interactions are mapped onto a self consistent field. The homogeneous nearest-neighbor Heisenberg ferromagnet has the mean-field Curie-temperature $T_c = (S + 1)zJ/3k_BS$, where S is the spin quantum number and z is the number of nearest neighbors.

The mean-field model is easily generalized to two or more sublattices. This site-resolved or lattice mean-field theory includes the case of nanomagnets, which have a very large number N of non-equivalent atomic sites or 'sublattices'. Since the J_{ij} form an N × N matrix, there are N coupled algebraic equations, and T_c is given by the largest eigenvalue of the matrix. J_{ij}/k_B [24, 36]. Using averaged exchange constants $< J_{ij}>$ fails to properly account for the spatial dispersion of the exchange. An extreme example is a mixture of two ferromagnetic phases with equal volume fractions but different Curie temperatures T_1 and $T_2 > T_1$. In the above approximation, $T_c = (T_1 + T_2)/2$, but in reality $T_c = T_2$ [36].

Note that mean-field theory is unable to describe the long-range correlations aspect of the problem, but the involved energy contributions are small, and the long-range features of the thermodynamics are not affected by the nanoscale effects [36].

In practice, it is difficult to distinguish the magnetism of particles or nanostructural features larger than about 1 nm from true ferromagnetism, because interatomic exchange ensures well-developed ferromagnetic correlations on a nanoscale. For example, when the radius of a particle is larger than a few interatomic distances, then the $M_s(T)$ curve is difficult to distinguish from a ferromagnet. Disordered two-phase nanostructures have a single common Curie temperature close to the Curie temperature of the phase with the strongest exchange coupling [5, 36, 37]. Similar considerations apply to multilayers [38–42] and to systems such as magnetic semiconductors [30]. Figure 4 illustrates that it is not possible to enhance the finite-temperature magnetization of a phase having a low Curie temperature by exchange-coupling it to a

phase with a high bulk Curie temperature [36]. This is clear contrast to the nanoscale improvement of extrinsic properties (§2.3.5).

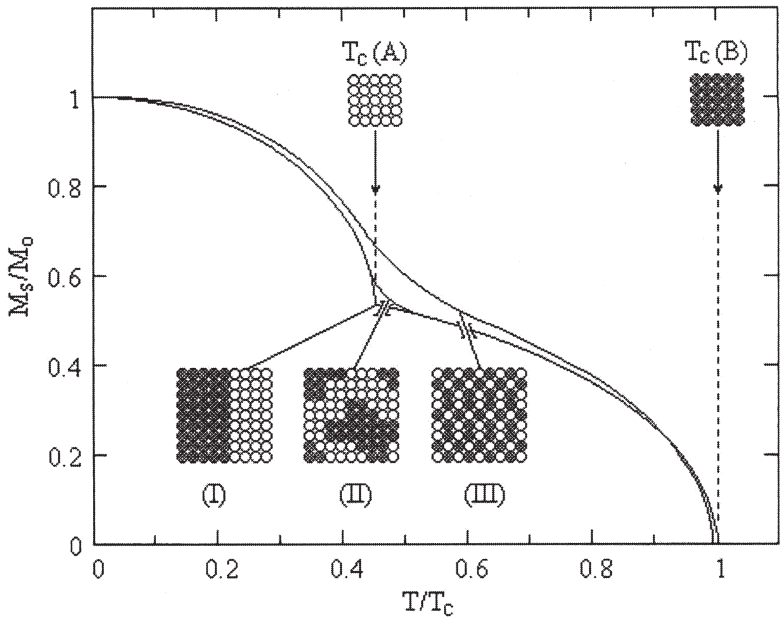

Figure 4. Spontaneous magnetization of inhomogeneous magnets: (I) macroscopic mixture, (II) nanostructure, and (III) alloy. In alloys and nanostructures, there is only one Curie temperature, although the $M_s(T)$ curves of nanostructures exhibit a two-phase like inflection whose curvature may be difficult to resolve experimentally [36].

Heisenberg interactions require well-defined atomic magnetic moments. where $\mathbf{S}^2 = S_o^2$. In insulators, $S_o^2 = S(S+1)$, whereas in metals, S_o is an expectation value and $\mathbf{S}/S_o$ has the character of a unit vector that describes the local magnetization direction. The assumption of a constant magnetic moment is often justified, because the total interatomic exchange per atom, of order 100 meV, tends to be much smaller than typical intra-atomic exchange energies of about 1000 meV [43]. Some exceptions are $L1_0$ magnets, where the 4d or 5d moments (Pd or Pt) are spin-polarized by the 3d atoms (Fe or Co) [44], and very weak itinerant ferromagnets, such as $ZrZn_2$ [16, 45]. Simplifying somewhat, the overall situation is intermediate between Heisenberg magnetism with stable local moments and a Stoner-like behavior where the moment vanishes at T_c. However, itinerant magnets such as Fe tend to be close to the

Heisenberg limit (Ch. 2), which establishes the spin-fluctuation picture of finite-temperature magnetism [16, 34].

2.1.5. Anisotropic Exchange

Heisenberg exchange is magnetically *isotropic*, that is, coherent rotation of a magnet's spin system does not change the Heisenberg exchange energy. For example, layered structures, such as YCo_5 and $L1_0$ magnets, tend to exhibit different intra- and interlayer interactions [44, 46], but the exchange does not depend on whether the magnetization is in-plane or normal to the layers. This exchange-bond anisotropy affects the spin structure of a magnet at both zero and nonzero temperatures. For example, it is the main source of spin noncollinearities encountered in elemental rare earths [33] and in magnetoresistive materials, such as NiMnSb [47]. Figure 1 shows some spin structures.

The bond anisotropy must not be confused with the relatively weak relativistic exchange anisotropies, which involve spin-orbit coupling and depend on the angle between the magnetization and the crystal axes. Examples are the exchange interactions assumed in the Ising and XY models, the magnetocrystalline anisotropy, and the unidirectional Dzyaloshinskii-Moriya exchange. For example: the exchange anisotropies $J_{xx} - J_{zz}$ and $J_{yy} - J_{zz}$ are small corrections to the isotropic exchange $J = (J_{xx} + J_{yy} + J_{zz})/3$. Another example is the *Dzyaloshinskii-Moriya* (or DM) interaction $\mathsf{H}_{DM} = -\frac{1}{2}\Sigma_{ij}\,\mathbf{D}_{ij}\cdot\mathbf{S}_i\times\mathbf{S}_j$, where the vector $\mathbf{D}_{ij} = -\mathbf{D}_{ji}$ reflects the local environment of the magnetic atom [48]. Net DM interactions require local environments with sufficiently low symmetry and occur, for example, in some crystalline materials, such as α-Fe_2O_3 (hematite), amorphous magnets, spin glasses, and magnetic nanostructures [5, 33, 48]. Micromagnetic noncollinearities, such as domain walls, also stem from relativistic effects, because they involve magnetocrystalline anisotropy, but their domain is nanoscale rather than atomic, and they are traditionally treated in the context of micromagnetism (§2.3). Compared to Heisenberg exchange, relativistic contributions are smaller by a factor of order α^2, where $\alpha = 1/137$ [5]. For example, typical DM canting angles are about 0.1°.

2.2. Magnetic Anisotropy

The dependence of the magnetic energy on the orientation of the magnetization with respect to the crystal axes is known as *magnetic anisotropy*. Permanent magnets need a high magnetic anisotropy, in order to keep the magnetization in a desired direction. Soft magnets are characterized by a very low anisotropy, whereas materials with intermediate anisotropies are used as magnetic recording media. In terms of the magnetization angles φ and θ,

the simplest anisotropy-energy expression for a magnet of volume V is $E_a = K_1 V \sin^2\theta$. This anisotropy is known as lowest-order (or second-order) *uniaxial* anisotropy, and K_1 is the first uniaxial anisotropy constant. It is often convenient to express anisotropies in terms of anisotropy fields. For example, the expression $E_a = K_1 V \sin^2\theta$ yields $H_a = 2\,K_1/\mu_o M_s$.

For magnets of low symmetry (orthorhombic, monoclinic, and triclinic), the lowest-order anisotropy energy is

$$E_a = K_1 V \sin^2\theta + K'_1 V \sin^2\theta \cos(2\phi) \qquad (5)$$

where K_1 and K'_1 are, in general, of comparable magnitude. This expression must also be used for magnets having a low-symmetry shape, such as ellipsoids with three unequal principal axes, for a variety of surface anisotropies, such as that of bcc (011) surfaces [49], and for nanoparticles with random surfaces. Equation 5 can also be written as $E_a = -\mathbf{M}\cdot\underline{\mathbf{K}}\cdot\mathbf{M}/M_s^2$, where $\underline{\mathbf{K}}$ is a 3×3 tensor. It obeys $\mathrm{Tr}\underline{\mathbf{K}} = 0$, and the two independent eigenvalues of $\underline{\mathbf{K}}$ correspond to K_1 and K'_1. Higher-order anisotropy expressions contain, in general, both uniaxial and planar terms. For example, $E_a/V = K_1 \sin^2\theta + K_2 \sin^4\theta$ contains second- and fourth-order uniaxial anisotrop terms and describes hexagonal and rhombohedral crystals [16, 50].

2.2.1. Origin of anisotropy

Figure 5 illustrates that there are two main sources of anisotropy: shape anisotropy and magnetocrystalline anisotropy. Shape anisotropy is important in magnetic nanostructures made from soft-magnetic materials, for example in Fe, Co, and Ni particles [16, 51] and in nanowires [52–55]. However, the anisotropy of most materials is of magnetocrystalline origin, reflecting the competition between electrostatic crystal-field interaction and spin-orbit coupling [7]. Note that the same mechanism is responsible for the quenching (or unquenching) of the orbital moment and for phenomena such as magnetic circular dichroism and anisotropic magnetoresistance.

For shape anisotropy, $K_1 = \mu_o(1 - 3D)M_s^2/4$, where D is the demagnetizing factor ($D = 0$ for long cylinders, $D = 1/3$ for spheres, and $D = 1$ for plates) [56]. It is important to note that shape anisotropy is limited to very small particles (§2.2). In large particles, shape anisotropy is destroyed by internal flux closure, indicated at the bottom of Fig. 5(a).

The crystal field [57], which contains both electrostatic and hopping contributions [58], acts on the orbits of the inner d and f electrons. That is, the electron orbits reflect the anisotropic crystalline environment, and adding spin-orbit coupling translates this anisotropic electron motion into magnetic anisotropy.

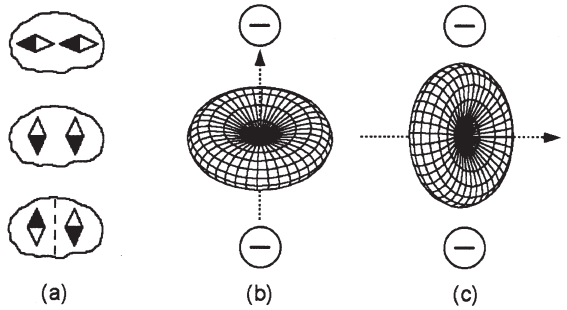

Figure 5. Physical origin of magnetic anisotropy: (a) compass-needle analogy of shape anisotropy and (b–c) magnetocrystalline anisotropy. In (b) and (c), the anisotropy energy is given by the electrostatic repulsion between the tripositive rare-earth ions and the negative crystal-field charges.

The magnitude of the magnetocrystalline anisotropy depends on the ratio of crystal-field energy and spin-orbit coupling. As a relativistic phenomenon, spin-orbit coupling is most pronounced for inner-shell electrons in heavy elements, such as rare-earth 4f electrons. This leads to a rigid or 'unquenched' coupling between spin and orbital moment, and the magneto-crystalline anisotropy is given by the relatively small electrostatic crystal-field interaction of the 4f charge clouds [59] with the crystal field [16, 60, 61]. This largely electrostatic mechanism, illustrated in Fig. 5(b) and 5(c), is responsible for the high room-temperature anisotropy of rare-earth permanent magnets, $K_1 \sim 10$ MJ/m^3 (see Appendix).

In 3d atoms, the spin-orbit coupling is much smaller than the crystal-field energy, and the magnetic anisotropy is a perturbative effect [7, 8, 16]. Typical second- and fourth-order transition-metal anisotropies are of the orders of 1 MJ/m^3 and 0.01 MJ/m^3, respectively. A manifestation of magnetocrystalline anisotropy is magnetoelastic anisotropy, where the crystal field is changed by mechanical strain [5, 16].

2.2.2. Surface and interface anisotropy

To realize second-order anisotropy, the atomic environment of the transition-metal atoms must have a sufficiently low symmetry [49, 62–65]. Figure 6 illustrates that this is often, but not always, the case for surface atoms. Magnetic surface anisotropy, first analyzed by Néel [62], is important in complicated structures and morphologies such as ultrathin transition-metal films [66], multilayers [67], rough surfaces [65], small particles [68], and surface steps

[69]. In a variety of cases it has been possible to calculate surface anisotropies from first principles [64, 67, 70–72]. The same is true for some other low-geometries, such as Fe wires embedded in Cu [73] and free-standing monatomic Co wires [74]. An interesting point is that surface anisotropies easily dominate the bulk anisotropy of cubic materials. From the tables in the appendix we see that bulk anisotropies are about two orders of magnitude smaller than lowest-order anisotropies. Due to the comparatively large number N_s of surface atoms of small particles, the surface contribution dominates the bulk anisotropy in particles smaller than about 3 nm, even if one takes into account that the net surface anisotropy is not necessarily linear in N_s but tends to scale as $N_s^{1/2}$ due to random-anisotropy effects.

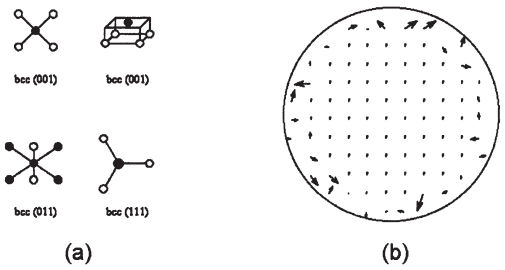

Figure 6. Surface anisotropy: (a) atomic origin and (b) realization in a nanoparticle. Lowest-order biaxial anisotropy is realized for bcc (011) but not for bcc (001) and bcc (111). The large surface-to-volume ratio of clusters leads to a comparatively strong diameter dependence of the intrinsic properties such as anisotropy [68] and magnetization.

Magnetocrystalline anisotropy is characterized by a pronounced temperature dependence [16, 61, 75–77]. For example, the leading rare-earth anisotropy contribution of permanent magnet intermetallics such as $SmCo_5$ and $Nd_2Fe_{14}B$ scales as $1/T^2$ [78]. The main reason is that typical anisotropy energies per atom are quite small, E_a ranging from less than 0.1 K to a few K. The realization of room-temperature anisotropy requires the support of the interatomic exchange field, which suppresses the switching of individual atomic spins into states with reduced anisotropy contributions [16,79,80].

Magnetocrystalline anisotropy is, essentially, a single-ion property, realized by embedding the atom in a metallic or nonmetallic crystalline environment [16, 58]. This must be compared to the popular Néel model [62], which ascribes anisotropy to pair interactions. Figure 7 illustrates the difference. The Néel model requires two interacting magnetic atoms (black), whereas the single-ion or crystal-field model amounts to hopping or crystal-field interactions with atoms that are not necessarily magnetic (white). The principal failure of the Néel model is seen by comparing Sm_2Fe_{17} and $Sm_2Fe_{17}N_3$, where the electronegative nitrogen is nonmagnetic but strongly affects the crystal field and changes the room-temperature anisotropy from –0.8 MJ/m^3 to 8.6 MJ/m^3 [16].

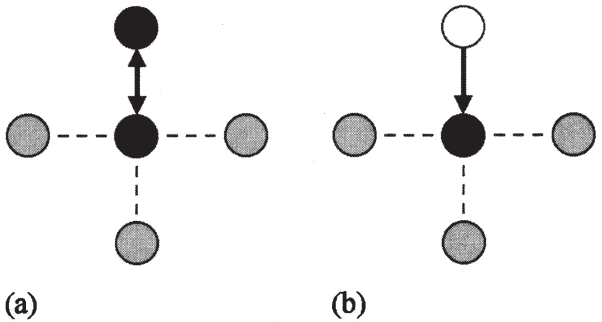

Figure 7. Models of magnetic anisotropy: (a) Néel model and (b) single-ion crystal-field model. Both models reproduce the correct symmetry, but (b) is physically more adequate for most systems.

2.2.3. Temperature dependence of anisotropy

In most materials, including nanostructures, the magnetocrystalline anisotropy is strongly decreases with increasing temperature. This is due to intra-atomic excitations. The strong temperature dependence of the leading rare-earth anisotropy contribution of hard-magnetic materials such as $SmCo_5$ and $Nd_2Fe_{14}B$ reflects intramultiplet excitations [16, 60, 61]. The excitations may be visualized as changes between Fig. 5(b) and 5(c). The figure indicates that these excitations compete against the crystal field. However, the crystal field is only one consideration; the main contribution is from the inter-sublattice exchange, which dominates thermal spin disorder.

For one-sublattice magnets, such as Fe and Co, the Akulov or Callen and Callen theory [81] relates the temperature dependence of the anisotropy to the spontaneous magnetization and yields M^3 and M^{10} power laws for uniaxial and cubic magnets, respectively. This theory has become popular far beyond its range of applicability [82] but is unable to describe structures such as rare-earth transition-metal magnets [16, 60], actinide magnets [83], and $L1_0$ type compounds [44, 84].

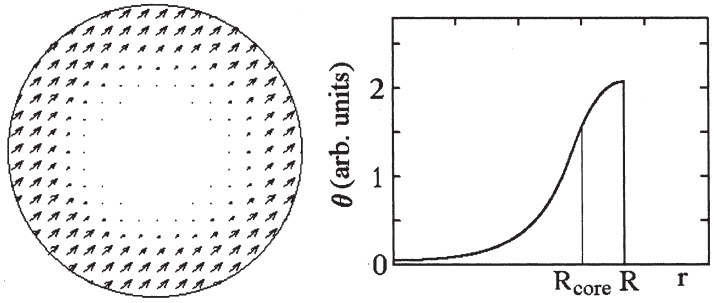

Figure 8. Nucleation mode in a small $L1_0$ particle. Due to reduced anisotropy at the surface, the reversal starts at the surface [89].

An interesting example is the finite-temperature magnetization of $L1_0$ magnets [44, 84, 85]. Elemental 4d/5d magnets, such as Pd and Pt, are exchanged-enhanced Pauli paramagnets, but in a ferromagnetic environment they are easily spin-polarized by neighboring 3d atoms. [86, 87]. The 4d/5d moment contributes little to the magnetization and Curie temperature, but it plays a key role in the realization of magnetic anisotropy, which is of the order of 5 MJ/m^3 at room temperature [88].

The temperature dependence of the anisotropy is reflects the collapse of the 4d/5d moment. The result of the calculation is an M^2 law [44], as compared to the Callen-Callen prediction M^3 and to refined simulations that yield an $M^{2.08}$ dependence [84]. By comparison, for uniaxial 3d magnets, such as Co and YCo_5, $m = 3$ [81], cubic and noncubic actinide magnets exhibit $m = 1$ [83], and for cubic 3d magnets, such as Fe and Ni, $m = 10$ [81]. Finally, rare-earth transition-metal intermetallics exhibit m ≈ 0, that is, the 4f sublattice anisotropy is largely independent of the leading 3d magnetization [16]. The exponents $m = 2$ and $m = 3$ are not very dissimilar [85], but the different physics—the crucial involvement of two sublattices—speaks in favor of $m = 2$. In fact, recent calculations by Mryasov *et al.* have yielded $m = 2.08$, amounting to a single-sublattice contribution of the order of 8%. As also pointed out in [84], the reduction of the number of 3d neighbors in magnetic nanoparticles has a very similar surface-anisotropy reduction effect.

2.3. Hysteresis of Magnetic Nanostructures

Magnetic anisotropy yields easy magnetization directions corresponding to local energy minima and energy barriers that separate the easy directions. On an atomic scale, the barriers are easily overcome by thermal fluctuations, but on

nanoscale or macroscopic length scales the excitations are usually too weak to overcome the barriers. This is observed as *magnetic hysteresis.*

Zeeman and selfinteraction (demagnetization) magnetic fields, interatomic exchange, and magnetic anisotropy all contribute to the rotation, which occurs on a mesoscopic scale and has been known historically as micromagnetism [90], although nanomagnetism would be a better name to characterize the involved length scales. Magnetic nanostructures exhibit a particularly rich extrinsic behavior, but even traditional 'microstructured' magnets exploit nanometer-scale features for performance optimization [91]. For example, the best room-temperature permanent magnets are now made from Nd-Fe-B [92], but as-cast samples with the correct stoichiometry exhibit a disappointingly low coercivity unless the grain-boundary structure is optimized by a specific heat treatment.

Figure 9 shows a typical hysteresis loop and illustrates how magnetic hysteresis is realized in real space. In the example of Fig. 9, the hysteresis reflects domain-wall pinning in a small particle. This means that magnetic domains are separated by domain walls (dotted lines) whose motion is impeded by real-structure defects or 'pinning centers' in the bulk or at the surface. Aside from a few basic hysteresis mechanisms, such as pinning, coherent rotation, curling, and localized nucleation, there exist many variations and combinations. The reason is the real-structure dependence of magnetic hysteresis, which makes it necessary to consider each material or each class of materials separately.

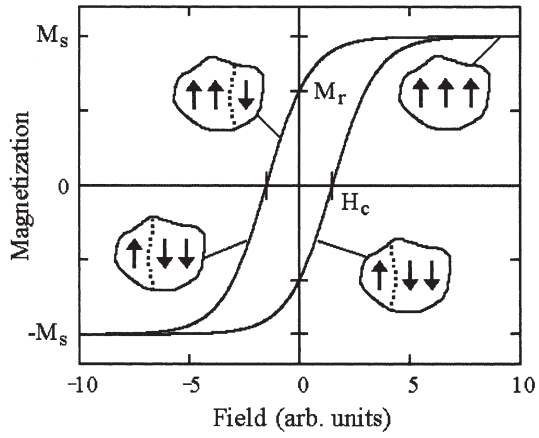

Figure 9. Magnetic hysteresis: origin and phenomenology of hysteresis. The coercivity of the particles shown in this figure is caused by domain-wall pinning at the grain- boundary phase.

2.3.1. Micromagnetic free energy

A key theoretical problem is to derive magnetization curves by simulating or modeling the magnet's nanostructure. This requires the determination of the local magnetization $\mathbf{M}(\mathbf{r})$, from which the hysteresis loop is obtained by averaging. The large strength of the intra-atomic exchange means that typical magnetization changes in magnetic solids are caused by moment rotations rather than by changes in the moments' magnitude. The result is the complicated nonlinear, nonequilibrium, and nonlocal problem of hysteresis. In addition, there is a strong real-structure influence. Properties related to hysteresis (extrinsic properties) are also known as micromagnetic properties [90], but this term is somewhat unfortunate, because most micromagnetic phenomena are nanoscale.

Hysteresis problems are usually treated on a continuum level [16, 90, 93]. Narrow-wall phenomena, which have been studied for example in rare-earth cobalt permanent magnets [94] and at grain boundaries [95, 96], involve individual atoms and atomic planes and lead to comparatively small corrections to the extrinsic behavior (§4.2). Furthermore, in contrast to the intrinsic phenomena considered in Section 2, which affect the spontaneous magnetization $M_s = |\mathbf{M}|$, micromagnetic phenomena are realized by local rotations of the magnetization vector. This is because typical micromagnetic energies are much smaller than the quantum-mechanical energy contributions that establish M_s.

To explain the hysteresis loop of magnetic materials one needs to trace the local magnetization $\mathbf{M}(\mathbf{r}) = M_s\mathbf{s}(\mathbf{r})$ as a function of the applied field H. This is achieved by considering the free-energy functional

$$F = \int \left\{ A\left[\nabla\left(\frac{\mathbf{M}}{M_s}\right)\right]^2 - K_1 \frac{(\mathbf{n}.\mathbf{M})^2}{M_s^2} - \mu_o \mathbf{M}\cdot\mathbf{H} - \frac{\mu_o}{2}\mathbf{M}\cdot\mathbf{H}_d(\mathbf{M}) \right\} dV \qquad (6)$$

Here $M_s(\mathbf{r})$ is the spontaneous magnetization, $K_1(\mathbf{r})$ is the first uniaxial anisotropy constant, $A(\mathbf{r})$ denotes the exchange stiffness, and $\mathbf{n}(\mathbf{r})$ is the unit vector of the local anisotropy direction. $\mathbf{H}$ is the external magnetic field, and $\mathbf{H}_d$ is the magneto static self-interaction field. The latter can be written as

$$\mathbf{H}_d(\mathbf{r}) = \frac{1}{4\pi}\int \frac{3(\mathbf{r}-\mathbf{r}')(\mathbf{r}-\mathbf{r}').\mathbf{M}(\mathbf{r}') - |\mathbf{r}-\mathbf{r}'|^2\mathbf{M}(\mathbf{r}')}{|\mathbf{r}-\mathbf{r}'|^5} dV' \qquad (7)$$

The *free*-energy character of F reflects the intrinsic or equilibrium temperature dependence of the parameters A, K_1, and M_s. Furthermore, these parameters are local parameters, because they depend on chemistry, crystal structure, and crystallite orientation.

Depending on the considered system, additional terms must be added to the micromagnetic equation. In lowest order, DM interactions amount to a random field $\Sigma_j(D_{ij,y}\mathbf{e}_x - D_{ij,x}\mathbf{e}_y)/2$ where the summation (or integration) over j includes all atomic neighbors; the resulting structure may be called a 'spin colloid.'

2.3.2. Micromagnetic length scales

Equation (6) yields not only the hysteresis loop but also the underlying micromagnetic spin structure. This includes features such as domains and domain walls. An aspect of great importance in nanomagnetism is the length scales on which these features are realized. Dimensional analysis of Eq. (6) yields two fundamental quantities, namely the wall-width parameter $\partial_o = \sqrt{A/K_1}$ and the exchange length $l_{ex} = \sqrt{A/\mu_o M_s^2}$. Other length and dimensionless parameters are derived from ∂_o and l_{ex}.

The *wall-width parameter* ∂_o varies from about 1 nm in extremely hard materials to several 100 nm in very soft materials. It determines the thickness $\partial_B = \pi\partial_o$ and energy $\gamma_w = 4K_1\partial_o$ of Bloch domain walls [13, 14, 97, 98], and describes the spatial response of the magnetization to local perturbations [95]. Essentially, the thickness of the walls is determined by the competition between exchange, which favors extended walls, and anisotropy, which favors narrow transition regions.

The *exchange length* l_{ex} is the length below which atomic exchange interactions dominate typical magnetostatic fields. It determines, for example, the particle cylinder radius $R_{coh} \sim 5l_{ex}$ above which curling is more favorable than coherent rotation {§2.3.3). It also yields the thickness of soft-magnetic films below which Néel walls are energetically more favorable than Bloch walls. For a broad range of ferromagnets, $l_{ex} \sim 2$ nm [16]. Note that the wall-width parameter ∂_o is sometimes interpreted as an exchange length. If this were a valid consideration, then ideally soft materials, where $K_1 = 0$ and $\partial_o = \infty$, would realize exchange coupling on a truly macroscopic scale. This is at odds with experiment.

Compared to domain-wall thicknesses, the determination of domain sizes tends to be very complicated [13, 14, 51, 93, 99–101]. This is because domains are caused by the strongly geometry- and size-dependent magnetostatic selfinteraction. An exception is the *critical single-domain radius*

$$R_{SD} = \frac{36\sqrt{AK_1}}{\mu_o M_s^2} \qquad (8)$$

of spherical particles, above which a two-domain state is more favorable than the single-domain state. This expression reflects the competition between domain-wall energy, $4\pi\sqrt{A K_1}\, R^2$, and gain in magneto static energy $\mu_o M_s^2 V/12$ [97]. In soft magnets, the critical single-domain size is only a few nanometers, but in very hard magnets it exceeds 1 μm.

It is important to emphasize that the critical single-domain radius is an equilibrium property. It involves the comparison of the of single-domain and multi-domain energies but is independent of the energy barriers separating the states. It determines, for example, the initial or virgin state after thermal demagnetization. By contrast, hysteresis is a nonequilibrium phenomenon caused by energy barriers. Furthermore, equilibrium domains are qualitatively different from the nonuniform (incoherent) magnetization states occurring during magnetization reversal (§2.3.3). The popular but incorrect equating of single-domain magnetism and coherent rotation has its origin in the focus on soft and semi-hard magnets in the first half of the 20th century.

Note that typical domain-wall widths are much smaller than the domains themselves. When the size of a magnetic particle is smaller than the domain-wall width ∂_B, as encountered for example in small soft-magnetic nanodots, then the distinction between domains and domain walls blurs, and the determination of the micromagnetic spin structure requires additional considerations [102]. One example is curling-type flux-closure or 'vortex' states.

2.3.3. Exact solutions

In small particles, the exchange is sufficiently strong to ensure that $\mathbf{M}(\mathbf{r})$ is constant throughout the magnet, that is, $\nabla\mathbf{M}$ in Eq. (6) is zero. Depending on the context, this regime is called coherent rotation, uniform rotation, or Stoner-Wohlfarth reversal [90, 103, 104]. For perfect uniaxial ellipsoids of revolution having the symmetry axis parallel to the external field $\mathbf{H} = H\mathbf{e}_z$, the energy (Eq. (6)) then becomes

$$\frac{F}{V} = K_1 \sin^2\theta + \frac{\mu_o}{2}(1-3D)\, M_s^2 \sin^2\theta - \mu_o M_s H \cos\theta \qquad (9)$$

Expanding this equation into powers into powers of θ and analyzing the stability of the local free-energy minimum at $\theta = 0$ yields the Stoner-Wohlfarth coercivity

$$H_c = \frac{2K_1}{\mu_o M_s} + \frac{1}{2}(1\text{-}3D)\, M_s \qquad (10)$$

This coercivity is a simple example of a nucleation field. In micromagnetism, the term nucleation refers to the instability of the remanent state in a reverse magnetic field $H_z = -H_N$. It does not necessarily imply localization effects [16, 93], although localized nucleation is frequently encountered in practice.

Increasing the radius of the particle leads to a transition from coherent rotation to curling. Figure 10 compares coherent-rotation and curling nucleation modes. Curling is favorable from the point of view of magnetostatic selfinteraction, because the vortex-like mode yields some flux closure, but it costs some exchange energy, because $\nabla\mathbf{M} \neq 0$. The derivation of the curling mode involves the exchange term in Eq. (6). After some calculation [16, 90, 93, 104] one obtains the nucleation-field coercivity

$$H_c = \frac{2K_1}{\mu_o M_s} - DM_s + \frac{c(D)\,A}{\mu_o M_s R^2} \qquad (11)$$

Here the radius R refers to the two degenerate axes of the ellipsoid, and c = 8.666 for spheres (D = 1/3) and c = 6.678 for needles (D = 0). In (11), the magneto static contribution, $-DM_s$, is always negative, in contrast to the term $(1 - 3D)M_s/2$ in (10). This means that there is no shape anisotropy in large magnets, although the exchange term in (11) partly compensates the absence of the exchange field [105].

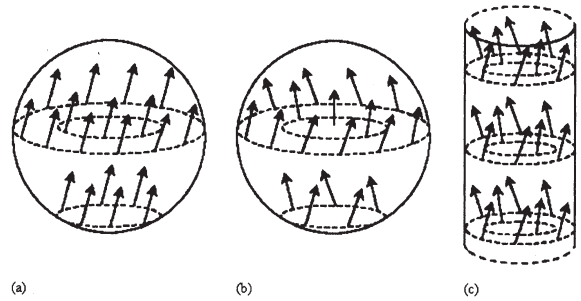

Figure 10. Nucleation modes in homogeneous magnets: (a) coherent rotation in a sphere, (b) curling in a sphere, and (c) curling in a cylinder. The arrows show the local magnetization $M = M_z e_z + m$, where e_z is parallel to the axis of revolution of the ellipsoid (cylinder).

Comparison of Eqs. (10) and (11) yields the radius R_{coh} for the transition from coherent rotation to curling. For $R < R_{coh}$, the exchange energy dominates, and the nucleation is realized by coherent rotation, whereas for $R > R_{coh}$ the nucleation behavior is dominated by flux closure and realized by curling. For spheres and wires (cylinders), one obtains $R_{coh} = 5.099\, l_{ex}$ and

$R_{coh} = 3.655\ l_{ex}$, respectively [16, 90, 93]. These radii are typically of the order of 10 nm. In thin films with perpendicular anisotropy ($D \approx 0$), curling occurs when the cross section of the films exceeds some value scaling as l_{ex} [9]. Note that R_{coh} is anisotropy-independent, in contrast to the critical single-domain radius R_{SD}. Since $R_{coh} \ll R_{SD}$ in hard magnets, there is a broad region $R_{coh} \approx 10$ nm and $R_{SD} \approx 1$ μm where hard-magnetic single-domain particles demagnetize incoherently. The popular but incorrect equating of single-domain magnetism and coherent rotation, as epitomized by the unfortunate term 'elongated single-domain particle' (ESD), has its origin in the focus on soft and semi-hard magnets in the first half of the 20th century.

2.3.4. Localized nucleation

The Stoner-Wohlfarth approach works fairly well for very small particles, where $\nabla \mathbf{M} = 0$ is a good approximation. However, it has been known for decades that neither the Stoner-Wohlfarth theory nor the additional consideration of the curling mode account for the coercivity of real materials. For example, the coercivity of optimized permanent magnets is only 20–40% of the anisotropy field $2K_1/\mu_o M_s$, and only a part of the discrepancy can be ascribed to the curling terms in Eq. (11). The reason is that real-structure imperfections make it impossible to consider the magnets as perfect ellipsoids of revolution.

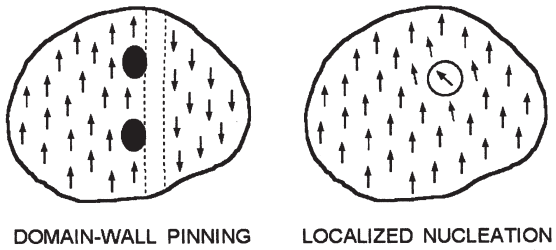

Figure 11. Pinning and nucleation. Pinning means that coercivity is created by trapping the domain wall at pronounced inhomogenities (pinning centers). In the absence of pinning centers, the coercivity is determined by the reversal field at which the original magnetization configuration becomes unstable (nucleation).

Figure 11 illustrates that there is an important distinction between domain-wall pinning and localized nucleation. Domain-wall pinning [15, 51, 99, 106], as illustrated in Fig. 11, requires relatively strong inhomogenities. For example, the high coercivity of Sm-Co-Cu-Zr permanent magnets reflects domain-wall pinning at a Cu-rich grain-boundary phase with strongly reduced anisotropy and domain-wall energy [5, 16, 77, 107, 108].

In nearly perfect magnets, pinning is unimportant, and the coercivity is determined by the stability of saturated (or nearly saturated) original magnetization state. This scenario is similar to coherent rotation and curling, except that a single nanoscale inhomogenity may initiate the magnetization reversal of a macroscopic magnet. This localized nucleation leads to strong reduction of H_N and solves Brown's paradox [90, 109], according to which the observed coercivities are often much smaller than predicted by (10).

To determine the nucleation field, we write the local magnetization as

$$\mathbf{M}(\mathbf{r}) = M_s \left(\sqrt{1 - m^2}\ \mathbf{e_Z} + \mathbf{m}(\mathbf{r}) \right) \tag{12}$$

where $\mathbf{m}$ is the perpendicular magnetization component ($|m| = \sin\theta$). Taking into account that $\mathbf{n} = e_z$ for aligned magnets, and expanding the free energy Eq. (6) into powers of $\mathbf{m}$ yields the quadratic expression

$$F = \int [\, A\, (\nabla \mathbf{m})^2 + K_1(\mathbf{r})\, \mathbf{m}^2 - \frac{1}{2} \mu_o\, M_s\, H\, \mathbf{m}^2] \, d\mathbf{r} \tag{13}$$

Here we have incorporated the magnetostatic selfinteraction into K_1 and H, which is a good approximation for many systems [5]. Eigenmode analysis of (13) yields the differential equation

$$A \nabla^2 m - \left(K_1(\mathbf{r}) + \frac{\mu_o}{2} M_s\, H \right) m = 0 \tag{14}$$

where we have assumed that A is constant throughout the magnet.

In terms of (14), imperfections appear as a modification of the local anisotropy $K_1(\mathbf{r})$ and lead to a nucleation-field and coercivity reduction [105, 110–112]. The solution of the nucleation problem is simplified by the fact that Eq. (14) has the same structure as the single-particle Schrodinger equation, $K_1(\mathbf{r})$ and H_c being the respective micromagnetic equivalents of $V(\mathbf{r})$ and E. Consider, for example, an imperfection in form of a cubic soft inclusion of volume L^3 in a hard matrix. The corresponding wave functions are particle-in-a-box states, and the nucleation field is [5]

$$H_c = \frac{6\, \pi^2 A}{\mu_o\, M_s\, L^2} \tag{15}$$

Analyzing this expression in terms of the exchange length reveals that imperfections are harmful if their size is comparable to or larger than a few nanometers.

In the past, nucleation fields such as Eq. (15) have been obtained for several cases: spherical particles in an infinitely hard matrix [110], small inclusions in a matrix of arbitrary anisotropy and exchange stiffness [105] [111], various types of multilayers [111, 113], and some core-shell and nanowire configurations [105, 114, 115]. For a discussion of the unphysical limit of very small inclusions, $L = 0$, see e.g. [5].

2.3.5. Nanostructured magnetic materials

There are various classes of magnetic materials (see Appendix), and both traditional materials and novel nanostructures exploit nanoscale phenomena [5]. An example of improving the performance of magnetic materials by nanostructuring is hard-soft permanent-magnet composites [16, 111, 116–120]. As analyzed in [16, 111], atomic-scale magnetism doesn't support substantial improvements of permanent magnets beyond existing intermetallics such as $SmCo_5$, Sm_2Co_{17}, and $Nd_2Fe_{14}B$. However, adding a soft phase to a hard phase in a suitable nanostructure can improve the permanent-magnet performance beyond that of the hard phase. In these structures, the hard phase acts as a skeleton to ensure a coercivity of the order of $H_c/2$, whereas adding the soft-magnetic high-magnetization phase enhances M_s and M_r [111]. This materials-by-design or 'metamaterials' approach makes it possible to produce materials not encountered in nature.

Note that isotropic single-phase and two-phase *permanent magnets* are comparatively easy to produce. Examples are nanocrystalline $Nd_2Fe_{14}B/Fe_3B$-Fe and $Sm_2Fe_{17}N_3$/Fe composites produced by melt-spinning [116] and mechanical alloying [121], respectively. However, the remanent magnetization M_r of randomly oriented grains with uniaxial anisotropy is only half the saturation magnetization M_s. Since the energy product of highly coercive permanent magnets scales as M_r^2, this amounts to a reduction of this key figure of merit by a factor of 4. Intergranular exchange improves the remanence by favoring parallel spin alignment in neighboring grains [116, 121–125]. However, this *remanence enhancement* is accompanied by a cooperative coercivity reduction, which limits the achievable energy product.

Magnetic nanostructures with c-axis alignment do not suffer from magnetization reduction due to random anisotropy. Examples of structures are multilayers [111, 113, 117], which are now widely associated with Kneller's concept of exchange-spring magnetism, and three-dimensional two-phase nanostructures [110, 111]. The model predictions by Skomski and Coey [16, 111] have been verified in Fe-Pt nanostructures [5, 119], but the experimental realization of high-performance multilayered [118, 120, 126–130] and granular [16, 95, 105, 111, 116, 119, 123–125, 131, 132] rare-earth transition-metal structures has remained a demanding challenge. The main reasons are difficulties in aligning the easy-axis of hard-phase grains, maintaining a uniform phase mixture on the scale of ~ 5 nm, and real-structure imperfections, which make it difficult to maintain coercivity.

3. MAGNETIZATION DYNAMICS

Magnetization processes are generally time-dependent, even if the external magnetic field is kept constant. For example, freshly magnetized permanent magnets lose a small fraction of their magnetization during the first few hours. In nanomagnets, the oscillation and relaxation times vary from less than one nanosecond to millions of years.

Atomic processes are very fast, so that intrinsic properties obey equilibrium statistics. An intermediate regime is characterized by typical magnetostatic and anisotropy energies per atom, about 0.1 meV, which correspond to times of order $\tau_o \sim 0.1$ ns. Examples are ferromagnetic resonance and related precession and damping phenomena. When energy barriers are involved, thermal excitations lead to a relatively slow relaxation governed by the Boltzmann-Arrhenius law [99, 133–137]

$$\tau = \tau_o \exp\left(\frac{E_a}{k_B T}\right) \tag{16}$$

This relation, known as the Néel-Brown law [135, 137], goes back to the 1930s [99]. Due to the exponential energy dependence, extrinsic equilibration times vary over many orders of magnitudes, from nanoseconds or milliseconds in superparamagnetic particles to decades in permanent magnets and recording media and millions of years in magnetic rocks.

3.1. Fundamental Equations

The time-dependent Schrodinger equation can, in principle, be used to predict the evolution of any physical system, but this method is not feasible in practice. First, the deterministic character of the Schrodinger equation forbids irreversible processes. Second, the many-body character of the Schrodinger equation, and the large number of degrees of freedom, such as lattice vibrations, complicate the description of real magnetic systems.

To make meaningful predictions about the relevant magnetic degrees of freedom, such as the position of a domain wall, one must treat the irrelevant atomic degrees of freedom as a heat bath, thereby introducing irreversibility. A simple classical analogue of this 'coarse graining' [5, 138–140] is a system of masses coupled by harmonic springs. The system has a recurrence time τ_{rec}

scaling as $1/\Delta\omega$, where $\Delta\omega$ is the system's smallest eigenfrequency difference. For any finite system the recurrence time is finite, but for an infinite number of degrees of freedom, corresponding to a heat bath, the solution yields a continuum of eigenvalues, $\Delta\omega = 0$ and $\tau_{rec} = \infty$.

The coarse-graining procedure simplifies the picture and provides the justification for various nonequilibrium approximations. One example is the Landau-Lifshitz equation

$$\frac{d\mathbf{M}}{dt} = \gamma \mathbf{M} \times \mathbf{H}_{eff} - \frac{1}{M_s^2 \tau_o} \mathbf{M} \times (\mathbf{M} \times \mathbf{H}_{eff}) \qquad (17)$$

where γ is the gyromagnetic ratio and $\mu_o \mathbf{H}_{eff} = -\partial E/\partial \mathbf{M}(\mathbf{r})$ is a local effective field [93, 141–143]. This equation—and similar relations, such as the Gilbert and Bloch-Bloembergen equations—describe the precession of the magnetization around $\mathbf{H}_{eff}$ and its relaxation towards the local or global energy minima associated with $\mathbf{H}_{eff}$. However, they are not able to describe thermally activated jumps over energy barriers.

There are several ways of describing thermal activation. Without loss of generality, we can restrict ourselves to a single magnetic degree of freedom s, such as a single magnetization angle or projection [144]. The relevant equation is the *Langevin* equation,

$$\frac{\partial s}{\partial t} = - \frac{\Gamma_o}{k_B T} \frac{\partial E}{\partial s} + \sqrt{2\Gamma_o}\, \xi(t) \qquad (18)$$

where $\xi(t)$ is a random force obeying $< \xi(t) > = 0$ and $< \xi(t)\, \xi(t') > = \delta(t - t')$. Physically, the force $-\partial E/\partial s$ drives the magnetization towards the local (free) energy minimum but competes with the random force $\xi(t)$. Figure 12 compares the two regimes describes by Eqs. (17) and (18). For the numerical realization of Landau-Lifshitz and Langevin equations see Ch. 4.

The probability distribution belonging to Eq. (18) obeys the diffusion-type magnetic *Fokker-Planck* equation [137, 140, 145]

$$\tau_o \frac{\partial P}{\partial t} = \frac{1}{k_B T} \frac{\partial}{\partial s} \left(P \frac{\partial E}{\partial s} \right) + \frac{\partial^2 P}{\partial s^2} \qquad (19)$$

This equation can also be written in form of a continuity equation, $\tau_o \partial P/\partial t = -\partial P/\partial s$. In equilibrium, $\partial P/\partial t = 0$ and $P = Z^1 \exp(-E(s)/k_B T)$, justifying the magnitude of the source term in Eq. (18). For energy barriers $E_a \gg k_B T$, Eq. (19) essentially reduces to Eq. (16) [145, 146].

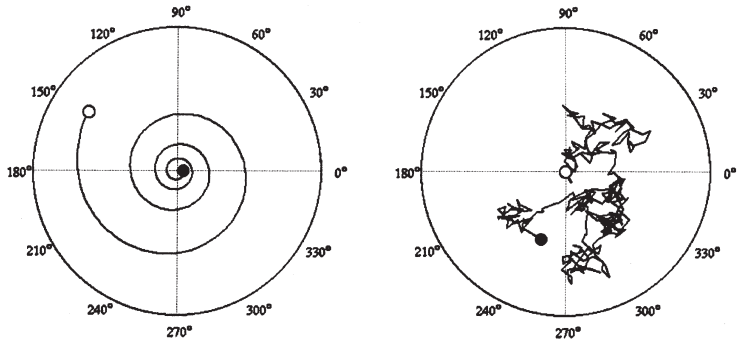

Figure 12. Magnetization dynamics of a nanoparticle: (a) damped precession and (b) random thermal motion. The curves are simulations for typical but not critical parameters, covering a time of order 0.1 ns. In both polar plots, the direction of the motion is from the white circles to the black circles.

A third and largely equivalent approach is the master or rate equation

$$\frac{\partial P(s)}{\partial t} = \int [W(s, s') P(s') - W(s', s) P(s)] ds' \qquad (20)$$

where the $W(s, s') = W(s' \rightarrow s)$ are transition rates. For example, describing the system by Fermi's golden rule yields

$$W_{ij} = \frac{2\pi}{\hbar} |\langle \Psi_i | V | \Psi_j \rangle|^2 \, \delta(E_i - E_j) \qquad (21)$$

where W_{ij} is the transition rate between two quantum states s_i and s_j. Specifying V relates the dynamics of a system to quantum mechanics, and Kramers-Moyal expansion of Eq. (20) with respect to small magnetization changes $s_i - s_j$ reproduces the diffusive Fokker-Planck equation (19).

3.2. Spin Waves in Nanostructures

Since Bloch's 1930 article on the temperature dependence of the spontaneous magnetization of ferromagnets [147], spin waves or magnons have attracted much attention in the solid-state and magnetism communities [50, 148, 149]. In particular, Bloch's spin-wave arguments indicate that there is no long-range isotropic ferromagnetism in two or fewer dimensions [10, 16,26, 35, 48, 147, 150]. In Bloch's original approach, the long-wavelength magnetization reduction due to spin waves is proportional to the integral $\int k^{d-3}\, dk$, which exhibits a long-wavelength divergence for $d \leq 2$. However, as explained in §2.1, the behavior of

experimental nanostructures is reminiscent of bulk ferromagnets. In a spin-wave picture, the energy of long-wavelength magnons is too small to interfere with the exchange energies that control moment formation and local magnetic order.

Ignoring the damping term in Eq. (17), the resonance is described by $d\mathbf{M}/dt = \gamma(\mathbf{M} \times \mathbf{H}_{eff})$. For homogeneously magnetized ellipsoids of revolution, the effective field is equal to the applied field $\mathbf{H} = H\,\mathbf{e}_z$ plus the anisotropy field $\mathbf{H}_a$, and the resonance problem is solved by the diagonalization of a 2 × 2 matrix. This uniform or ferromagnetic resonance (FMR) yields resonance frequencies determined by [17]

$$\omega^2 = \gamma^2 (H + H_{ax} - H_{az})(H + H_{ay} - H_{az}) \tag{22}$$

where $\mathbf{e}_x$ and $\mathbf{e}_y$ correspond to the principal axes of the 2 × 2 matrix. In systems with rotational symmetry, such as perfect nanowires aligned parallel to the external magnetic field, this equation degenerates into

$$\omega = \gamma (H + 2\,K_{eff}/\mu_o M_s) \tag{23}$$

where $K_{eff} = K_1 + \mu_o M_s^2/4$.

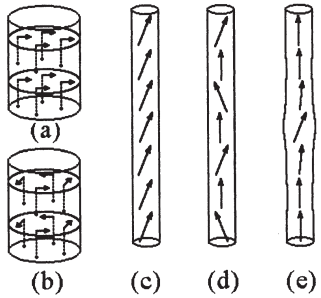

Figure 13. Spin-wave modes in nanowires: (a) is the coherent mode ($k_\perp = 0$) and (b) is of the curling type. When $k_\perp \gg 1/R$, then the perpendicular spin waves are essentially superpositions of plane waves $\exp(ik_x x)$ and $\exp(ik_y y)$. Since the diameter of typical nanowires is much larger than interatomic distance, there are many excited perpendicular modes, and the finite-temperature magnetization $M_s(T)$ is reminiscent of bulk magnets.

Recent research has largely focused on spin-wave excitations in perfect nanostructures [151–156]. In addition, real-structure effects have been considered [5, 153]. In macroscopic systems, the superposition of individual lines leads to a line broadening due to real-structure inhomogenities and field gradients. In nanostructures, the superposition of resonance lines is

a poor approximation, because the modes are coupled by interatomic exchange. Since the nucleation mode is essentially an $\omega = 0$ spin-wave mode [93], the considerations of §2.3.4 carry over to the problem of spin waves in real nanostructures [5, 153].

Figure 13 shows various types of spin-wave modes in long nanowires. In very thin nanowires, where $R < R_{coh}$, curling-type modes can be ignored [55, 114], and the perpendicular magnetization components obey $M_x = M_s\, m(z) \cos(\omega t)$ and $M_y = M_s\, m(z) \sin(\omega t)$. Note that both curling and the radial spin-wave quantization in terms of Bessel functions [153] leads to very high level splittings and can be ignored in lowest order. The function $m(z)$ obeys

$$-2A\frac{d^2m}{dz^2} + \left(2\,K_{eff}(z) + \mu_o M_s H - \frac{\omega}{\gamma}\right) m = 0 \tag{24}$$

For $\omega = 0$, this equation reduces to (14), whereas $dm/dz = 0$ reproduces (23). Mathematically, Eq. (24) is a well-known random-potential eigenvalue problem, which can be solved numerically or by transfer-matrix methods [5, 153].

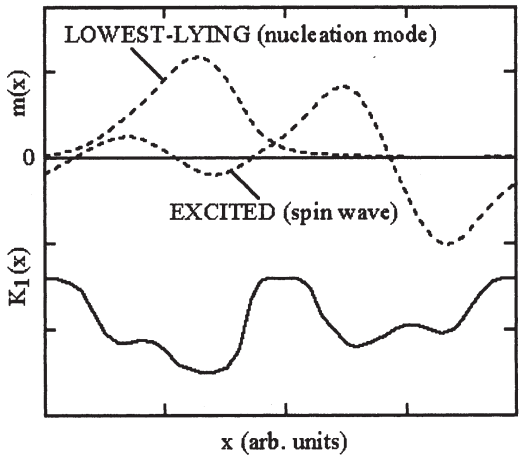

Figure 14. Localization of spin-wave modes with k vectors along the wire axis. All modes are localized, but the localization length is smallest for low-lying modes.

Figure 14 shows some examples. An interesting point is that all modes are localized [105], as one expects from the quantum-mechanical analog of a one-dimensional electron gas in a random potential [157]. Alternatively, from a localized 'tight-binding' point of view, micromagnetic delocalization can

be interpreted as a tunneling through hard-magnetic regions. The localization length depends on ω and is largest for high frequencies.

A major source of real-structure inhomogenities are wire-thickness fluctuations and polycrystallinity, and geometrical features at wire ends [54, 55, 114, 158]. As expected from §2.3.4, the localization of the modes is accompanied by a coercivity reduction [54, 55, 114].

3.3. Magnetic Viscosity

The extrinsic time dependence of the magnetization is known as *magnetic viscosity*. The magnetic viscosity determines, for example, the stability of the information stored in magnetic recording media [159] and the time-dependent decay of the remanent magnetization of permanent magnets. From a thermodynamic point of view, this is the origin of hysteresis, and similar magnetic freezing processes are the superparamagnetic freezing of small particles and ferrofluids [160–162] and Spill glasses [33, 48, 140, 163, 164]. A related effect is the dependence of the coercivity on the sweep rate dH/dt of the external magnetic field [16, 99, 134]. As illustrated in Fig. 15, both effects are caused by thermal activation and involve jumps over (free) energy barriers. Thermally activated jumps yield only small corrections, because typical energy barriers in ferromagnets are much larger than $k_B T$.

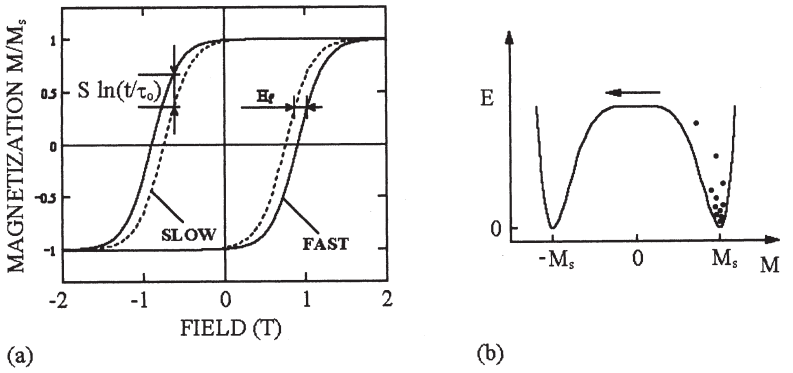

Figure 15. Dynamic hysteresis-loop effects: (a) magnetic viscosity and (b) sweep-rate dependence. The sweep-rate dependence amounts to a fluctuation-field [165] or sweep-rate correction to the static coercivity H_{co}.

Experiment shows that the time dependence of the magnetization is often *logarithmic* rather than exponential [16, 99, 136, 159, 166, 167]. As pointed out long ago [99], a logarithmic time dependence is obtained by averaging

over exponential relaxation processes $M(t) = -M_s + 2M_s \exp(-t/\tau)$. The key assumption is that the distribution of the relaxation time or reflects an energy-barrier barrier distribution much larger than $k_B T$.

In [99], a rectangular energy-barrier distribution was used, but this is an unnecessary and rather complicated assumption. In fact, introducing an energy-barrier distribution $P(E_a)$ leads to the integral

$$M(t) = -M_S + 2M_S \int_{-\infty}^{\infty} P(E_a)\, e^{-(t/\tau_o)\exp(-E_a/k_B T)}\, dE_a \qquad (25)$$

and to [5, 168]

$$M(t) = M(t') - 2 k_B T P(0) \ln(t/t') M_s \qquad (26)$$

where t and t' are two arbitrary reference times. Phenomenologically, the logarithmic law is often written as $M(t) = M(t) - S\ln(t/t')$, where S is the magnetic-viscosity constant. Note that the logarithmic law breaks down for $t = \infty$. An expression with improved asymptotics is [168]

$$M(t) = 2 M_S (t/\tau_O)^{-k_B T/E_O} - M_S \qquad (27)$$

However, since $(x^{\varepsilon} - 1) = \varepsilon \ln x$ for small exponents, this expression is not very different from the logarithmic law.

An important aspect of magnetic viscosity is its *field dependence*. For example, $S(H)$ tends to exhibit a maximum near the coercivity. This reflects the close relationship between the energy-barrier distribution and the irreversible part χ_{irr} of the susceptibility, and leads to $S = \chi_{iir} S_v$, where the viscosity parameter S_v is only weakly field-dependent [5, 133, 159, 167, 169–172].

An effect closely related to magnetic viscosity is the dependence of the coercivity on the sweep rate $\eta = dH/dt$: H_c is largest for high sweep rates, that is, for fast hysteresis-loop measurements (Fig. 15). Sweep-rate and magnetic-viscosity dynamics have the same origin, but there is a very simple way of deriving a relation for the sweep-rate dependence. Let us assume that the energy barriers exhibit a power-law dependence

$$E_a(H) = K_o V_o \left(1 - \frac{H}{H_o}\right)^m \qquad (28)$$

where K_o, V_o, and m are micromagnetic parameters. This law is not restricted to aligned Stoner-Wohlfarth particles, where $K_o = K_1$, $V_o = V$, and $m = 2$, but also describes a broad range of pinning and nucleation mechanisms.

Putting Eq. (28) into Eq. (16) and identifying H with reverse field at which the magnetization state escapes the local energy minimum yields [134, 140]

$$H_c = H_o\left(1 - \left(\frac{k_B T}{K_o V_o}\ln(\tau/\tau_o)\right)^{1/m}\right) \tag{29}$$

where $\tau \sim 1/\eta$. A slightly more sophisticated calculation, first published in the 1960s [134] and popularized by Sharrock more than ten years ago [173], yields a relatively unimportant factor of ln2 = 0.693, which is usually incorporated into τ_o.

An experimental approach to analyze the resulting sweep-rate dependence of the coercivity is to exploit the phenomenological relation [159]

$$H_c(\eta) = H_c(\eta_o) + \frac{k_B T}{M_s V^*}\ln\left(\frac{\eta}{\eta_o}\right) \tag{30}$$

Linearizing Eq. (30) with respect to $\ln(\eta/\eta_o) = -\ln(\tau/\tau_o)$ [16]

$$V^* = \frac{m}{2}\left(\frac{25 k_B T}{K_o V_o}\right)^{1-1/m} V_o \tag{31}$$

This equation shows that the activation volume V^* is only loosely related to the 'physical' or 'Barkhausen' volume V_o. Furthermore, V_o is not necessarily the volume of a single particle-due to cooperative and localization effects its may be smaller or larger than the particle volume.

The exponent m cannot be regarded as a fitting parameter but depends on the symmetry of the system. In most cases, $m = 3/2$ [16, 140, 158, 166, 167, 174, 175], but $m = 2$ for highly symmetric systems, such as aligned Stoner-Wohlfarth particles. In particular, the $m = 3/2$ law is realized for misaligned Stoner-Wohlfarth particles and for most domain-wall pinning mechanisms [5]. Experimental values of m tend to vary between 1.5 to 2 [136, 158]. Linear laws, where $m = 1$, are sometimes used in simplified models, but so far it hasn't been possible to derive them from physically reasonable energy landscapes [5, 16, 176]. The same is true for dependences such as $1/H - 1/H_o$ [177], where series expansion yields an $m = 1$ power law.

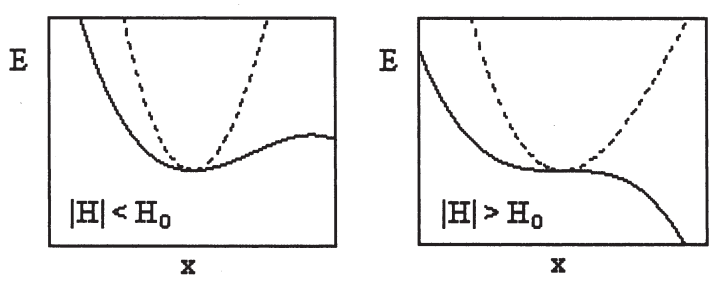

Figure 16. Multidimensionality of the coercivity problem: Only the trajectory corresponding to the lowest-lying mode contributes to the switching.

It is important to keep in mind that there are many possible magnetization-reversal modes, including modes whose energy scales as $1/H$, but only the lowest-lying one—that with the smallest nucleation or propagation field H_o—is of importance for the magnetic-viscosity and sweep-rate corrections to zero-temperature magnetization reversal [5, 37, 93, 175]. Other reversal modes are not forbidden, but typical energy-barrier differences are much larger than $k_B T$ and make the associated 'giant fluctuations' very unlikely. Fig. 16 illustrates the underlying energy landscape by schematically comparing the lowest-lying mode (solid line) with an excited mode (dashed line). The thermodynamically preferred direction is along the solid line, whereas excited modes are suppressed by a Boltzmann factor $\exp(-\Delta E_a/k_B T)$. An explicit example is shown in Fig. 17. The pinning and giant-fluctuation mechanisms (a) and (b) obey $m = 3/2$ power and $1/H$ laws, respectively. At low temperatures, magnetization reversal requires $E_a = 0$, and Eq. (29) yields some finite coercivity $H_c = H_o$. By contrast, the activation energy for the droplet configuration of Fig. 17(b), described by an $1/H$ law, amounts to the unphysical prediction of an infinite zero-temperature anisotropy.

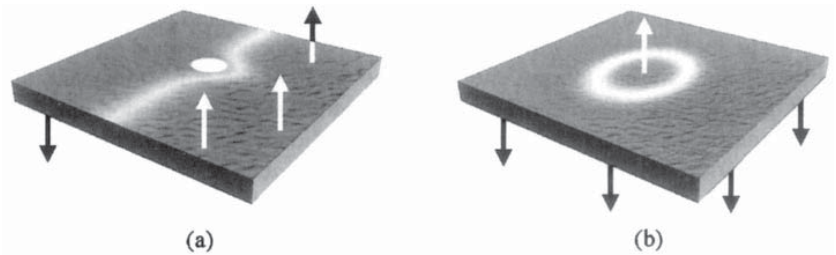

Figure 17. Coercivity mechanisms in thin films: (a) power-law type pinning and (b) $1/H$-type spontaneous reversal.

The above consideration requires energy barriers much larger than $k_B T$, as encountered in most nanostructures. An exception is very small particles, where $K_o V_o$ is comparable to $k_B T$, exhibit a rapid decay of the magnetization, which is known as super paramagnetism [160, 178, 179]. Defining superparamagnetism by a waiting time of τ = 100 s yields the zero-field stability condition $K_o V_o / k_B T \geq 25$, where $K_o V_o / k_B T \equiv \xi$ is referred to as the stability parameter. Thermal stability for 10 years corresponds to ξ = 40 [55, 159]. Other exceptions are atomic wires and monatomic thin films, where corrections to the power law of Eq. (28) must be considered.

Equation (29) amounts to a $T^{1/m}$ dependence of the coercivity [16], but this is only one consideration. In many cases, the biggest contribution to the temperature dependence of the coercivity is from the intrinsic $K_1(T)$ behavior (§2.2.3). This mechanism amounts to explicit changes in the energy landscape. The leading contribution is static, involving thermal averages $< K_1(T) >$, but there is also a dynamic correction, with fluctuating saddle-point energies.

4. CASE STUDIES

4.1. Magnetic Localization and Cooperativity

From an atomic point of view, all nanostructures are cooperative, because interatomic exchange ensures well-defined local spin correlations. In other words, nanoscale magnetization processes involve blocks of spins rather than individual spins. The sizes of the correlated regions are nanoscale, in agreement with the analysis in §2.3, but vary from system to system [180]. The coherent-rotation and curling modes are delocalized, that is, they extend throughout the magnet. Delocalized magnetization states are favorable from the point of view of interatomic exchange, because the magnetization gradient is small. However, exchange is not the only consideration, because local variations of the magnetization cost some exchange energy but may be favorable from the point of view of local anisotropy inhomogenities.

The localization length and the coercivity reduction depend on the ratio of exchange and anisotropy energies. The stronger the anisotropy inhomogenity, the smaller the localization length L, and for a soft inclusion in a very hard matrix, as considered in §2.3, the localization length reduces to the size of the inclusion. For zero disorder, that is, for perfect ellipsoids of revolution, the localization length goes to infinity and the reversal degenerates into coherent rotation.

Cooperative effects are of great importance in advanced technology. For example, in high-density magnetic recording media they lead to the formation of interaction domains, which may improve the thermal stability but reduce the storage density. In permanent magnets the vanishing of the two-phase shoulders in hysteresis loops can be considered as a cooperative effect [180, 181], as is the above discussed low coercivity of soft-magnetic random-anisotropy magnets (Ch. 13). Similar arguments apply to finite-temperature phenomena (Fig. 18). On a local scale, the spin alignment remains largely ferromagnetic but thermal excitations and local perturbations break the cooperativity on a nanoscale.

Weakly interacting particles and grains are noncooperative. In this limit, one can use micromagnetic mean-field theories, the Preisach model [182, 183], and approaches based on Wohlfarth's remanence relation [184], such as Henkel [185], delta-M [186, 187], and delta-H [188] plots. When the interactions exceed a certain threshold, the behavior of the magnet changes from noncooperative to cooperative. In this regime, the above-mentioned approaches are no longer applicable. For example, the exchange field of strongly coupled small particles exceeds 100 T. In the mean-field approximation, this field adds to the external field and yields an unphysically high coercivity [122, 180]. In reality, the strong exchange field does not translate into a high coercivity, and cooperativity may even reduce the coercivity. This is because two strongly interacting particles behave like one particle, and there is no point in adding any strong internal interaction to the external field.

A rough criterion for the applicability of interaction-field models is obtained from the slope of the hysteresis loop at coercivity, $\chi_c = dM(H_c)/dH$. When M_s/χ_c is smaller than the interaction field, then the behavior of the magnet is governed by cooperative effects [180]. In terms of Fig. 14, this is not surprising, because broad switching-field distributions correspond to pronounced inhomogenities and therefore to strong localization.

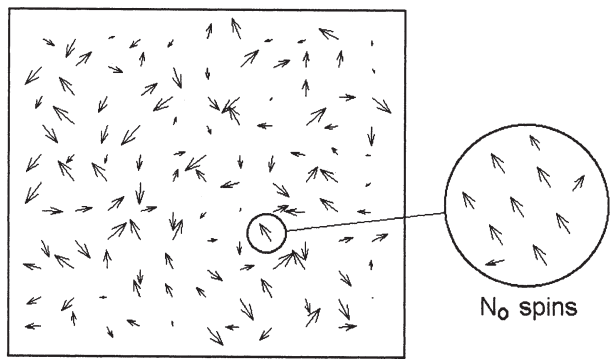

Figure 18. Cooperative spin blocks. When the size N of the particle becomes too big, then thermal activation leads to the formation of cooperative units of size N_o.

4.2. Narrow-Wall and Grain-Boundary Effects

Typical domain walls are smooth and extend over many interatomic distances. However, deviations from this continuum picture occur in very hard materials (narrow walls), at grain boundaries and in the case of geometrical constraints. Narrow-wall phenomena, which have been studied for example in rare-earth cobalt permanent magnets [189] and at grain boundaries [95, 96], involve individual atoms and atomic planes and lead to comparatively small corrections to the extrinsic behavior.

The nanoscale spin structure at grain boundaries and nanojunctions affects the performance of permanent magnets, magnetic recording media, soft magnets, and structures for spin electronics (Chs. 11–14). In permanent magnets, it is often necessary to maximize [16, 111] or minimize the intergranular exchange, depending on the desired reversal mechanism. Strong intergranular exchange reduces the coercivity of isotropic soft-magnetic nanostructures but is undesired in magnetic recording, where it negatively affects the storage density [159, 190], and the resistance of spin-electronic structures depends on the local magnetization at interfaces and at junctions [95, 96, 191]. Some aspects of grain-boundary magnetism were anticipated long ago [94, 111, 113, 192], but polycrystalline granular interfaces and constrained domain walls was first investigated have been investigated only recently.

We start from Eq. (6) and restrict ourselves to linear case of weakly textured systems, so that we can use a linear approach similar to that in §2.3.4 [5]. The corresponding equation for the local easy axis is $\mathbf{n}(\mathbf{r}) = \sqrt{1 - a^2(\mathbf{r})}\, e_z + \mathbf{a}(\mathbf{r})$, where $\mathbf{a}(\mathbf{r})$ is the transverse vector components of $\mathbf{n}$. Linearization yields [5]

$$F = \int \left[A\,(\nabla \mathbf{m})^2 + K_1\,(\mathbf{m} - \mathbf{a})^2 + \frac{1}{2}\,\mu_0\, M_s\, H\, \mathbf{m}^2 \right] \mathbf{dr} \qquad (32)$$

As in Eq. (32), the magneto static selfinteraction is incorporated into K_1 and H. To minimize F with respect to $\mathbf{m}(\mathbf{r})$ we exploit that the minimum of any functional $F = \int f\, dV$ is given by the functional derivative $\delta F/\delta \mathbf{m}(\mathbf{r}) = 0$. Explicitly,

$$\frac{\delta F}{\delta \mathbf{m}(\mathbf{r})} = -\nabla \left(\frac{\partial f}{\partial\, \nabla \mathbf{m}(\mathbf{r})} \right) + \frac{\partial f}{\partial \mathbf{m}(\mathbf{r})} \qquad (33)$$

so that

$$-\nabla(A \nabla \mathbf{m}) + \left(K_1 + \frac{1}{2}\, M_s\, H \right) \mathbf{m} = K_1\, \mathbf{a}(\mathbf{r}) \qquad (34)$$

This equation means that the polycrystalline easy-axis disorder $\mathbf{a}(\mathbf{r})$ acts as a random inhomogenity.

The term $\nabla(A \nabla \mathbf{m})$ reflects due to local character of exchange stiffness $A(\mathbf{r})$ [111]. For sharp phase boundaries, the exchange term reduces to the boundary condition

$$\left(A(\mathrm{x}) \frac{\partial m}{\partial x} \right) \Big|_{\mathrm{x_0}-\varepsilon} = \left(A(\mathrm{x}) \frac{\partial m}{\partial x} \right) \Big|_{\mathrm{x_0}+\varepsilon} \qquad (35)$$

Figure 19 illustrates the physical meaning of this boundary condition. A jump in $A(\mathrm{x})$ leaves the magnetization continuous but yields a change in the slope of the perpendicular magnetization component $m(\mathrm{x})$. The solutions of (34) are exponentially decaying in the adjacent grains and nearly linear in the interface region [95, 96].

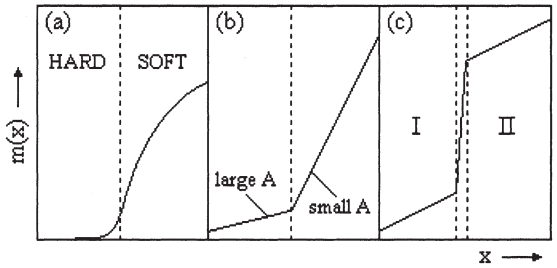

Figure 19. Boundary conditions and exchange: (a) hard-soft interface with common A, (b) interface between two ferromagnetic phases with different A, and (c) quasi-discontinuous magnetization due to strongly reduced exchange between grains I and II. Note that the perpendicular magnetization component $m(\mathrm{x})$ can be interpreted as a magnetization angle.

When the exchange stiffness in the grain-boundary region is much lower than that of the two adjacent phases, then one encounters a *quasi-discontinuity* of the magnetization [95, 96], as shown in Fig. 19(c). Experimentally, reduced interface exchange reflects real-structure features such as impurity atoms diluting the interatomic exchange, oxide layers covering the grains, and interface amorphization. Putting calculated spin structures $m(\mathrm{x})$ into Eq. (32) and evaluating the integral as a function of the misalignment vector a yields the *effective intergranular exchange*

$$J_{\text{eff}} = S_o \sqrt{A\,K_1}\,\frac{1}{1+\dfrac{\pi\,D\,A}{2\,\delta_B A'}} \tag{36}$$

where S_o is the interface area [96]. This equation shows that the effective exchange can never be larger than the value $S_o(AK_1)^{½}$, which scales as Bloch-wall energy of a perfect magnetic crystal. By contrast, the widely used 'hard interface' approach, which assigns bonds of strength $J' \approx A'/a$ to each of the $N \approx S_o/a^2$ adjacent pairs of atoms, yields $J_{\text{eff}} \approx S_o A'/a$ and generally overestimates the effective exchange. The explicit dependence of A on R modifies the scaling behavior to $L \sim R^{(2-d)/(4-d)}$ and $H_c \sim R^{d/(4-d)}$. Note that the exponent for L changes sign for $d \leq 2$. In this case, the exchange through the grain boundary is not able to overcompensate the reduction of grain size, and there are no correlated grains with $L > R$.

In the limit of vanishing anisotropy, the situation remains similar to Fig. 19(c), because the anisotropy changes the curvature of the magnetization angle. Solving Eq. (34) for this special case yields the following relation for the effective exchange A_{eff}: $D/A_{\text{eff}} = (D - t)/A + t/A^{\text{I}}$. This is of practical importance in soft magnetism (Ch. 13).

In a *layer-resolved* or atomic analysis, the ∇ operator in Eqs. (32–35) must be replaced by magnetization-angle differences, but a comparison with the continuum solution [95, 96] reveals only minor corrections due to the discrete nature of the layers. Note, however, that the layer resolved anisotropies and exchange constants may deviate from the respective bulk values.

Using the integral $\int(\nabla\mathbf{M})^2 dx \approx M_s^2 \int(\nabla\mathbf{m})^2 dx$ as a crude measure to gauge the spin-dependent scattering ability of an interface we find that the scattering is maximized for interface thicknesses of the order of $D = \delta_o A'/A$. Compared to the relatively small Bloch-wall scattering, where $\int(\nabla\mathbf{m})^2 dx \approx 1/\delta_o$, the maximum scattering is enhanced by a factor A/A'. Unfortunately, strong reductions of A' are likely to negatively affect the spin injection through the boundary region, thereby reducing the magnetoresistance. Another way of enhancing the scattering is using very hard materials, where δ_o is small, but this requires large fields to switch the magnetization direction [95].

Random-anisotropy contributions, as epitomized by the $\mathbf{a}(\mathbf{r})$-term in Eq. (34), are an important aspect of nanomagnetism, but their detailed treatment goes beyond the scope of this chapter. Some aspects of random-anisotropy magnetism will be treated in the chapter on soft magnets, and we also recommend reading or consulting the rich original and review literature [16, 48, 116, 124, 189, 193–197].

4.3. Quantum Entanglement between Magnetic Nanodots

The use of quantum bits or qubits is a promising way to meet the ever-increasing needs of information technology, with various advantages over classical information processing in areas such as factorization and cryptography [198–200]. Most systems considered at present, including magnetic structures such as spin chains and spin clusters, operate at very low temperatures, typically much smaller than 1 K [201–203]. The smallness of Bohr's magneton, $\mu_B/k_B = 0.672\ K/T$, makes it difficult to exploit magnetic fields [201] at temperatures significantly above 1 K. Superconducting magnets are able to create fields much larger than 1 T (10 kOe), but they are very cumbersome and may not establish a practical alternative. Exchange anisotropy is, in principle, an alternative [201, 202], but lowest-order exchange is isotropic, and the exchange anisotropies are small and difficult-to-realize relativistic corrections to the isotropic exchange (§2.1.5). However, anisotropic magnetic nanodots may open the door for quantum information processing significantly above 4.2 K. The idea is to exploit the quantum entanglement of the dots [204].

Figure 20 shows a model of two coupled and generally nonequivalent magnetic nanodots or clusters. The dots' total spins S and S' can be written as $S = N\,S_o$ and $S' = N'S'_o$, where N and N' are the respective numbers of magnetic atoms per dot. The Hamiltonian of the first dot contains the Zeeman energy $-g\mu_o\mu_B H\hat{S}_z$ and the anisotropy term

$$H_a = -\frac{K\,N}{3\,S^2}\,(3\,\hat{S}_z^2 - \hat{S}^2) \tag{37}$$

where K is the anisotropy energy per atom. Analog relations exist for the second dot. There are two reasons for considering nonequivalent dots. First, real nanomagnets tend to have imperfections, and it is extremely difficult to produce identical dots. Second, nonequivalent dots may exhibit unequal level spacings, which simplifies the addressing of well-defined quantum states, for example in resonance experiments.

The energy difference (level spacing) between the lowest two eigenvalues of Eq. (37), $KN(2S–1)/S^2$, determines the maximum operation temperature. We assume that the two dots are coupled by a Heisenberg-type exchange J. It may be realized, for example, by Ruderman-Kittel-Kasuya-Yosida (RKKY) interaction through a substrate or medium [27, 205], by a nanojunction, or by magnetostatic interactions. The interaction is the basis for entanglement of the dots' wave functions, which is a precondition for quantum computing.

Schrodinger's *verschränkung* or entanglement is a quantum effect, without classical analog and plays a key role in quantum computing [201, 206].

In a simple two-particle interpretation, the spin of a given particle depends on that of the second spin (entangled state) or is independent of the second particle's spin (nonentangled or separable state). In the Schmidt decomposition, the two-particle wave function can be written as

$$|\Psi\rangle = \alpha|00\rangle + \beta|01\rangle + \gamma|10\rangle + \delta|11\rangle \qquad (38)$$

For example, the four maximally entangled Bell states are proportional to $|00\rangle \pm |11\rangle$ and $|01\rangle \pm |10\rangle$. To describe low-temperature entanglement, we construct a Schmidt basis from the two lowest-lying single-dot states $|0\rangle$ and $|1\rangle$, which have $|S_z| = S$ and $|S_z| = S - 1$, respectively. Note that higher excitations do not affect the entanglement of the low-lying states [204]. The right-hand side of Fig. 20 illustrates the physical meaning of this basis for ferromagnetic and antiferromagnetic couplings.

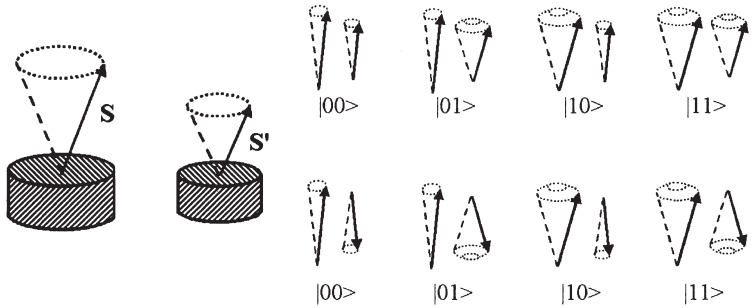

Figure 20. Quantum states of interacting nanodots. The dots (left) may be coupled ferromagnetic (top right) or antiferromagnetic (bottom right). The labels $|0\rangle$ and $|1\rangle$, denote states where $|m| = S$ and $|m| = S - 1$, respectively.

A quantitative entanglement measure is the concurrence C [206]. For nonentangled (separable) states, $C = 0$, whereas the maximally entangled Bell states exhibit $C = \pm 1$. The concurrence is obtained by evaluating the matrix elements of the total Hamiltonian and examining the lowest-lying two-dot eigenstates [204, 207]. It depends on whether the coupling is ferromagnetic (FM, $J > 0$) or antiferromagnetic (AFM, $J < 0$). The ferromagnetic ground state and the first two excited AFM states are separable, that is, $C = 0$. Nonzero entanglement is encountered in the AFM ground state and between low-lying ferromagnetic excitations [204].

Figure 21 shows C as a function of the anisotropy of the second dot. The entanglement of the low-lying FM excitations exhibits a resonant peak whose width depends on the interaction strength. Since a local magnetic field shifts the

single-dot energies, a field gradient can be used to tune the entanglement. The dashed line in Fig. 21 shows that there is no peak in the antiferromagnetic case.

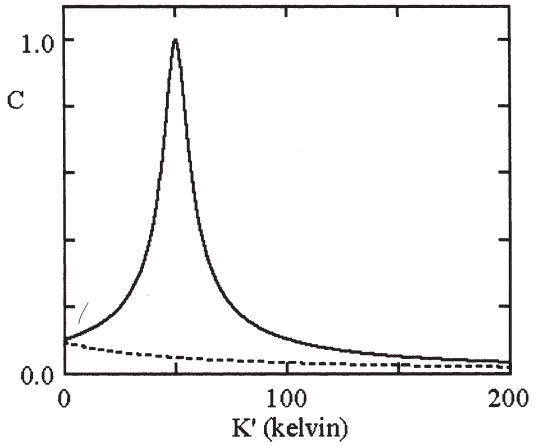

Figure 21. Entanglement as a function of the anisotropy K' of the second dot. The solid and dashed lines denote FM and AFM couplings, respectively. The parameters are $S_o = S_o' = 1$, $N = 1000$, $N' = 1100$, $K = 50$ K, and $J = 0.005$ K. For simplicity, $H = 0$ and $H' = 0$. The FM maximum is a resonance effect involving $|01\rangle$ and $|10\rangle$ states; there is no similar resonance in the AFM case.

Since the basic level splitting and the maximum operating temperature are proportional to the anisotropy, it is necessary to use dots with high magnetocrystalline anisotropy. Dots with shape anisotropy and semihard dots, such as Co, cannot be used, because they correspond to temperatures of one kelvin or less.

Much higher temperatures are achievable for $SmCo_5$ and other highly anisotropic materials. However, typical hard-magnetic materials have temperature-dependent anisotropies that are maximized at or above room temperature [16, 77]. Little work has been done to optimize anisotropies at low temperatures, although it is known that some compounds with $T_c < 300$ K have huge anisotropies of 100 to 1000 MJ/m^3 [83, 208].

In sufficiently small dots, the maximum operating temperature is proportional to the magnetocrystalline anisotropy of the dot material. An upper limit of the operation temperature is significantly above 10 K but probably below 100 K. An upper limit to the temperature above which spin-wave-like excitations and magnetic domains destroy quantum coherence is given by the energies of the lowest-lying spin-wave states. They scale as Aa^3/L^2, where A is the exchange or spin-wave stiffness of the dot material [16], a is the interatomic distance, and L is the dot size. For typical materials at temperatures signif-

icantly higher than 1 K, this quantity does not exceed a few nanometers. In bigger dots, low-lying spin-waves excitations have energies comparable to K and decoherence occurs very fast.

5. CONCLUDING REMARKS

From a scientific point of view, nanomagnetic effects are intermediate between atomic-scale magnetism and macroscopic phenomena but cannot be reduced to a mixture of the two limits. The main reason is the competing involvement of relativistic interactions, which give rise to an additional length scale of a_o/α = 7.25 nm. Intrinsic properties, such as spontaneous magnetization, Curie temperature, and magnetocrystalline anisotropy, reflect comparatively strong quantum-mechanical and spin-orbit interactions. They are realized on atomic length scales and therefore well-defined for nanostructures. However, surface and interface contributions such as magnetic interface anisotropy may be strong and outweigh bulk contributions on a nanoscale. Extrinsic properties, such as coercivity, are realized on larger length scales and exhibit a pronounced real-structure dependence.

A particularly subtle property is the Curie temperature, which describes the onset of ferromagnetism and involves long-range thermodynamic fluctuations. In a strict sense, the Curie temperature of finite bodies is zero, but the nonequilibrium character of practically encountered magnetic phenomena and the low energy differences associated with long-range thermodynamic fluctuations mean that particles or grains larger than about 1 nm., are virtually indistinguishable from true ferromagnets. For this reason, nanostructuring cannot be used to improve the Curie temperature.

It is important to distinguish between equilibrium and nonequilibrium extrinsic properties. The equilibrium behavior of magnetic nanostructures, as epitomized by the critical single-domain radius, is largely irrelevant to hysteresis. For example, in highly anisotropic rare-earth transition-metal permanent magnets, the critical single-domain size is of the order of 1 μm, but this does not mean that the magnetization reversal in such a particle is Stoner-Wohlfarth like. In fact, the reversal is localized, and typical coercivities are realized on a length scales of a few nanometers.

From a structural point of view, surfaces, interfaces, and bottlenecks (junctions) have a strong impact on nanomagnetism. One issue is that exchange at grain boundaries affects the coupling between nanograins and, indirectly, the extrinsic properties of the structures. Reduced grain-boundary exchange leads to a quasi-discontinuity of the magnetization. By contrast, anisotropy changes in the grain-boundary region have no major effect on the spin structure.

Intrinsic properties correspond to a very fast equilibrium, whereas the equilibration times of extrinsic properties cover a broad range, from a about one nanosecond in soft-magnetic resonance experiments and to millions of years in magnetic rocks. The slowest mechanism is thermally activated jumps over nanomagnetic energy barriers. This results in small low-temperature magnetic-viscosity corrections to the leading intrinsic contribution. Since the phase-space trajectories responsible for thermally A activated magnetization reversal are very close to static trajectories, 'giant' thermodynamic fluctuations involving arbitrary modes can safely be ignored.

In conclusion, magnetic nanostructures exhibit various scientifically interesting and technologically important deviations from bulk and thin-film magnets. For example, there is a resonant quantum entanglement of the low- lying states of coupled hard-magnetic dots, which may be exploited in future quantum-information processing above 4.2 K. Some others examples, mentioned or elaborated here and throughout this book, are the energy-product enhancement in nanostructured two-phase magnets whose hard-magnetic performance is improved by adding a soft-magnetic phase, multilayered and granular spin-valve structures, nanostructured soft magnets, and magnetic recording media. The principles and mechanisms outlined in this chapter make it possible to realize properties not achievable in single-phase bulk and thin-film materials, and form a basis for future experimental, technological and theoretical developments in the fascinating field of nanomagnetism.

Acknowledgement

This work has benefited from discussions with P. A. Dowben, A. Kashyap, R. D. Kirby, A. Y. Istomin, A. F. Starace, D. Leslie-Pelecky, S.-H. Liou, J.-P. Liu, K. D. Sorge, and D. J. Sellmyer. The underlying research is supported by NSF MRSEC, DARPA/ARO, DOE, ONR, AFOSR, the W. M. Keck Foundation, and CMRA.

References

[1] W. Heisenberg, Z. Phys. **49**, 619 (1928).

[2] F. Bloch, Z. Phys. **57**, 545 (1929).

[3] J. C. Slater, Phys. Rev. **49**, 537-545 (1936).

[4] E. C. Stoner, Proc. Roy. Soc. **A165**, 372 (1938).

[5] R. Skomski, J. Phys.: Condens. Matter **15**, R841 (2003).

[6] R. Skomski, J. Magn. Magn. Mater. **272-276**, 1476 (2004).

[7] F. Bloch and G. Gentile, Z. Phys. **70**, 395 (1931).

[8] H. Brooks, Phys. Rev. **58**, 909 (1940).

[9] R. Skomski, H.-P. Oepen, and J. Kirschner, Phys. Rev. B **58**, 3223 (1998).

[10] E. Ising, Z. Phys. **31**, 253 (1925).

[11] J. C. Slater, Rev. Mod. Phys. **25**, 199 (1953).

[12] Depending on the context, the real structure is also known as the defect structure, morphology, or metallurgical microstructure. For example, see: D. Sander, Rep. Prog. Phys. **62**, 809 (1999).

[13] F. Bloch, Z. Phys. **74**, 295 (1932).

[14] L. Landau and E. Lifshitz, Phys. Z. Sowjetunion **8**, 153 (1935).

[15] M. Kersten, Z. Phys. **44**, 63 (1943).

[16] R. Skomski and J. M. D. Coey, "Permanent Magnetism," Institute of Physics, Bristol 1999.

[17] C. Kittel, "Introduction to Solid State Physics," Wiley, New York 1986.

[18] B. T. Thole, P. Carra, F. Sette, and G. van der Laan, Phys. Rev. Lett **68**, 1943 (1992).

[19] Both spin-orbit coupling and Zeeman interactions are obtained as terms in the Pauli expansion of the Dirac equation.

[20] F. Cyrot-Lackmann, J. Phys. Chem. Solids **29**, 1235 (1968).

[21] V. Heine, Solid State Phys. **35**, 1 (1980).

[22] A. P. Sutton, "Electronic Structure of Materials," Oxford University Press, Oxford 1993.

[23] M. C. Desjonqueres and D. Spanjaard, "Concepts in Surface Physics," Springer, Berlin 1993.

[24] J. S. Smart, "Effective Field Theories of Magnetism," Saunders, Philadelphia 1966.

[25] N. H. Duc, T. D. Hien, D. Givord, J. J. M. Franse, and F. R. de Boer, J. Magn. Magn. Mater. **124**, 305 (1993).

[26] N. W. Ashcroft and N. D. Mermin, "Solid State Physics," Saunders, Philadelphia 1976.

[27] R. Skomski, Europhys. Lett. **48**, 455 (1999).

[28] R. Skomski, R. F. Sabiryanov, and S. S. Jaswal, J. Appl. Phys. **87**, 5890 (2000).

[29] J. A. De Toro, M. A. López de la Torre, J. M. Riveiro, J. Bland, J. P. Goff, and M. F. Thomas, Phys. Rev. B **64**, 224421 (2001).

[30] D. J. Priour Jr., E. H. Hwang, and S. Das Sarma, Phys. Rev. Lett. **92**, 117201 (2004).

[31] J. M. D. Coey, M. Venkatesan, and C. B. Fitzgerald, Nature Materials **2**, 173 (2005).

[32] D. C. Mattis, "Theory of Magnetism," Harper and Row, New York 1965.

[33] K. Moorjani and J. M. D. Coey, "Magnetic Glasses," Elsevier, Amsterdam 1984.

[34] P. Fulde, "Electron Correlations in Molecules and Solids," Springer, Berlin 1991.

[35] J. M. Yeomans, "Statistical Mechanics of Phase Transitions," University Press, Oxford 1992.

[36] R. Skomski and D. J. Sellmyer, J. Appl. Phys. **87**, 4756 (2000).

[37] R. Skomski, D. Leslie-Pelecky, R. D. Kirby, A. Kashyap, and D. J. Sellmyer, Scripta Mater. **48**, 857 (2003).

[38] H. R. Ma and C. H. Tsai, Solid State Commun. **55**, 499 (1985).

[39] W. Maciejewski and A. Duda, Solid State Commun. **64**, 557 (1987).

[40] H. K. Sy, Phys. Lett. A **120**, 203 (1987).

[41] W. Maciejewski, IEEE Trans. Magn. **26**, 213 (1990).

[42] R. W. Wang and D. L. Mills, Phys. Rev. B **46**, 11681 (1992).

[43] There are a few exceptions, such as very weak itinerant ferromagnets (for example $ZrZn_2$) and low-spin high-spin transition in *fcc* iron.

[44] R. Skomski, A. Kashyap, and D. J. Sellmyer, IEEE Trans. Magn. **39**, 2917 (2003).

[45] P. Mohn, "Magnetism in the Solid State," Springer, Berlin 2003.

[46] A. Kashyap, R. Skomski, R. F. Sabiryanov, S. S. Jaswal, and D. J. Sellmyer, IEEE Trans. Magn. **39**, 2908 (2003).

[47] R. Skomski and P. A. Dowben, Europhys. Lett. **58**, 544 (2002).

[48] K.-H. Fischer and A. J. Hertz, "Spin Glasses," University Press, Cambridge 1991.

[49] D. Sander, R. Skomski, C. Schmidthals, A. Enders, and J. Kirschner, Phys. Rev. Lett. **77**, 2566 (1996).

[50] M. Farle, Rep. Prog. Phys. **61**, 755 (1998).

[51] R. M. Bozorth, "Ferromagnetism," van Nostrand, Princeton, New Jersey 1951.

[52] H. Zeng, M. Zheng, R. Skomski, D. J. Sellmyer, Y. Liu, L. Menon, and S. Bandyopadhyay, J. Appl. Phys. **87**, 4718 (2000).

[53] G. T. A. Huysmans and J. C. Lodder, J. Appl. Phys. **64**, 2016 (1988).

[54] M. Zheng, R. Skomski R, Y. Liu, and D. J. Sellmyer, J. Phys.: Condens. Matter. **12**, L497 (2000).

[55] D. J. Sellmyer, M. Zheng, and R. Skomski, J. Phys.: Condens. Matter **13**, 433 (2001).

[56] J. A. Osborn, Phys. Rev. **67**, 351 (1945).

[57] H. Bethe, Ann. Physik, **3**, 133 (1929).

[58] C. J. Ballhausen, "Ligand Field Theory," McGraw-Hill, New York 1962.

[59] M. T. Hutchings, Solid State Phys. **16**, 227 (1964).

[60] J. F. Herbst, Rev. Mod. Phys. **63**, 819 (1991).

[61] J. M. D. Coey (ed.), "Rare-earth Iron Permanent Magnets," University Press, Oxford 1996.

[62] L. Néel, J. Phys. Radium **15**, 225 (1954).

[63] Y. Millev, R. Skomski, and J. Kirschner, Phys. Rev. B **58**, 6305 (1998).

[64] J. A. C. Bland and B. Heinrich (eds.), "Ultrathin Magnetic Structures I," Springer, Berlin 1994.

[65] M. T. Johnson, P. J. H. Bloemen, F. J. A. den Broeder, and J. J. de Vries, Rep. Prog. Phys. **59**, 1409 (1996).

[66] U. Gradmann, in: "Handbook of Magnetic Materials," Vol. **7**, Ed. K. H. J. Buschow, Elsevier, Amsterdam 1993, p. 1.

[67] R. H. Victora and J. M. McLaren, Phys. Rev. B **47**, 11583 (1993).

[68] M. Jamet, W. Wernsdorfer, C. Thirion, D. Mailly, V. Dupuis, P. Melinon, and A. Pérez, Phys. Rev. Lett. **86**, 4676 (2001).

[69t D. S. Chuang, C. A. Ballentine, and R. C. O'Handley, Phys. Rev. B **49**, 15084 (1994).

[70] J. G. Gay and R. Richter, Phys. Rev. Lett. **56**, 2728 (1986).

[71] G. H. O. Daalderop, P. J. Kelly, and M. F. H. Schuurmans, Phys. Rev. B **42**, 7270 (1990).

[72] D.-S. Wang, R.-Q. Wu, and A. J. Freeman.-Phys. Rev. B **47**, 14932 (1993).

[73] M. Eisenbach, B. L. Gyorffy, G. M. Stocks, and B. Újfalussy, Phys. Rev. B **65**, 144424 (2002).

[74] M. Komelj, C. Ederer, J. W. Davenport, and M. Fähnle, Phys. Rev. B **66**, 140407 (2002).

[75] J.-F. Hu, I. Kleinschroth, R. Reisser, H. Kronmillller, and Sh. Zhou, phys. stat. sol. (a) **138**, 257 (1993).

[76] E. Lectard, C. H. Allibert, and R. Ballou, J. Appl. Phys. **75**, 6277 (1994).

[77] K. Kumar, J. Appl. Phys. **63**, R13 (1988).

[78] R. Skomski, J. Appl. Phys. **83**, 6724 (1998).

[79] J. M. Cadogan, J. P. Gavigan, D. Givord, and H. S. Li, J. Phys. F: Met. Phys. **18**, 779 (1988).

[80] J. F. Liu, T. Chui, D. Dimitrov, and G. C. Hadjipanayis, Appl. Phys. Lett. **85**, 3007 (1998).

[81] E. R. Callen and H. B. Callen, Phys. Rev., **129**, 578 (1963).

[82] J. B. Staunton, S. Ostanin, S. S. A. Razee, B. L. Gyorffy, L. Szunyogh, B. Ginatempo, and E. Bruno, Phys. Rev. Lett. **93**, 257204 (2004).

[83] R. Skomski, J. Appl. Phys. **91**, 8489 (2002).

[84] O. N. Mryasov, U. Nowak, K. Guslienko, and R. Chantrell, Europhys. Lett. **69**, 805 (2005); O. N. Mryasov, U. Nowak, K. Guslienko, and R. Chantrell, unpublished (2004).

[85] N. H. Hai, N. M. Dempsey, and D. Givord, IEEE Trans. Magn. **39**, 2914 (2003).

[86] G. H. O. Daalderop, P. J. Kelly, and M. F. H. Schuurmans, in: "Ultrathin magnetic structures I," Eds.: J. A. C. Bland and B. Heinrich, Springer, Berlin 1994, p. 40.

[87] G. Brown, B. Kraczek, A. Janotti, T. C. Schulthess, G. M. Stocks, and D. D. Johnson, Phys. Rev. B **68**, 052405 (2003).

[88] R. A. McCurrie, "Ferromagnetic Materials—Structure and Properties," Academic Press, London 1994.

[89] J. Zhou, R. Skomski, K. D. Sorge, and D. J. Sellmyer, Scripta Materialia (2005) (in press).

[90] W. F. Brown, "Micromagnetics," Wiley, New York 1963.

[91] The prefix 'micro' originates from the Greek word *μικρός*, meaning "small" but not implying any well-defined length scale.

[92] M. Sagawa, S. Fujimura, N. Togawa, H. Yamamoto, and Y. Matsuura, J. Appl. Phys. **5**5, 2083 (1984); M. Sagawa, S. Hirosawa, H. Yamamoto, S. Fujimura and Y. Matsuura, Jpn. J. Appl. Phys. **26**, 785 (1987).

[93] A. Aharoni, "Introduction to the Theory of Ferromagnetism," University Press, Oxford, 1996.

[94] H. R. Hilzinger and H. Kronmüller, phys. stat. sol. (b), **54**, 593, (1972).

[95] R. Skomski, in: "Spin Electronics," Eds.: M. Ziese and M. J. Thornton, Springer, Berlin 2001, p. 204.

[96] R. Skomski, H. Zeng, and D. J. Sellmyer, IEEE Trans. Magn. **37**, 2549 (2001).

[97] C. Kittel, Rev. Mod. Phys. **21**, 541 (1949).

[98] D. J. Craik and R. S. Tebble, Rep. Prog. Phys. **24**, 116 (1961).

[99] R. Becker and W. Döring, "Ferromagnetismus," Springer, Berlin 1939.

[100] S. Chikazumi, "Physics of Magnetism," Wiley, New York 1964.

[101] M. Hehn, K. Ounadjela, J. Bucher, F. Rousseaux, D. Decanini, B. Bartenlian, and C. Chappert, Science **272**, 1782 (1995).

[102] R. Skomski, A. Kashyap, K. D. Sorge, and D. J. Sellmyer, J. Appl. Phys. **95**, 7022 (2004).

[103] E. C. Stoner and E. P. Wohlfarth, Phil. Trans. Roy. Soc. A240, 599 (1948). reprinted in IEEE Trans. Magn. MAG-27, 3475 (1991).

[104] A. Aharoni, Rev. Mod. Phys. **34**, 227 (1962).

[105] R. Skomski, J. P. Liu, and D. J. Sellmyer, Phys. Rev. B **60**, 7359 (1999).

[106] R. Skomski, J. Zhou, A. Kashyap, and D. J. Sellmyer, IEEE Trans. Magn. **40**, 2946 (2004).

[107] J. Zhou, R. Skomski, C. Chen, G. C. Hadjipanayis, and D. J. Sellmyer, Appl. Phys. Lett. **77**, 1514 (2000).

[108] J. Zhou, A. Kashyap, Y. Liu, R. Skomski, and D. J. Sellmyer., IEEE Trans. Magn. **40**, 2940 (2004).

[109] W. F. Brown, Rev. Mod. Phys. **17**, 15 (1945).

[110] R. Skomski, phys. stat. sol. (b) **174**, K77 (1992).

[111] R. Skomski and J. M. D. Coey, Phys. Rev. B **48**, 15812 (1993).

[112] R. Skomski, J. Appl. Phys. **83**, 6503 (1998).

[113] S. Nieber and H. Kronmüller, phys. stat. sol. (b) **153**, 367 (1989).

[114] R. Skomski, H. Zeng, M. Zheng, and D. J. Sellmyer, Phys. Rev. B **62**, 3900 (2000). [115] R. Skomski, J. Appl. Phys. **91**, 7053 (2002).

[116] R. Coehoorn, D. B. de Mooij, J. P. W. B. Duchateau, and K. H. J. Buschow, J. de Physique **49**, C-8 669 (1988).

[117] E. F. Kneller and R. Hawig, IEEE Trans. Magn. **27**, 3588 (1991).

[118] I. A. Al-Omari and D. J. Sellmyer, Phys. Rev. B **52**, 3441 (1995).

[119] J. P. Liu, C. P. Luo, Y. Liu, and D. J. Sellmyer, Appl. Phys. Lett. **72**, 483 (1998).

[120] E. E. Fullerton, J. S. Jiang, C. H. Sowers, J. E. Pearson, and S. D. Bader, Appl. Phys. Lett. **72**, 380 (1998).

[121] J. Ding, Y. Liu, P. G. McCormick, and R. Street, J. Appl. Phys. **75**, 1032 (1994).

[122] E. Callen, Y. J. Liu, and J. R. Cullen, Phys. Rev. B **16**, 263 (1977).

[123] K.-H. Müller, J. Schneider, A. Handstein, D. Eckert, P. Nothnagel, and H. R. Kirchmayr, Mat. Sci. Eng. **A133**, 151 (1991).

[124J A. Manaf, P. A. Buckley, and H. A. Davies, J. Magn. Magn. Mater. **128**, 302 (1993).

[125] H.-W. Zhang, B.-H. Li, J. Wang, J. Zhang, Sh.-Y. Zhang, and B.-G. Shen, J. Phys. D: Appl. Phys. **33**, 3022 (2000).

[126] E. E. Fullerton, S. J. Jiang, and S. D. Bader, J. Magn. Magn. Mater. **200**, 392 (1999).

[127] M. Sawicki, G. J. Bowden, P. A. J. de Groot, B. D. Rainford, J. M. L. Beaujour, R. C. C. Ward, and M. R. Wells, Phys. Rev. B **62**, 5817 (2000).

[128] R. J. Astalos and R. E. Camley, Phys. Rev. B **58**, 8646 (1998).

[129] G. C. Hadjipanayis, J. Magn. Magn. Mater. **200**, 373 (1999).

[130] G. J. Bowden, J. M. L. Beaujour, S. Gordeev, P. A. J. de Groot, B. D. Rainford, and M. Sa-

wicki, J. Phys.: Condens. Matter **12**, 9335 (2000).

[131] Y. Yoshizawa, S. Oguma, and K. Yamauchi, J. Appl. Phys. **64**, 6044 (1988).

[132] R. Coehoorn, D. B. de Mooij, and C. de Waard, J. Magn. Magn. Mater. **80**, 101 (1989).

[133] R. Street and J. C. Wooley, Proc. Phys. Soc. **A62**, 562 (1949).

[134] E. Kneller, in: "Handbuch der Physik XIII/2: Ferromagnetismus," Ed.: H. P. J. Wijn, Springer, Berlin 1966, p. 438.

[135] L. Néel, Ann. Geophys. **5**, 99 (1949).

[136] E. Kneller, "Ferromagnetismus," Springer, Berlin 1962.

[137] W. F. Brown, Phys. Rev. **130**, 1677 (1963).

[138] R. Zwanzig, Phys. Rev. **124**, 983 (1961).

[139] H. Mori, Prog. Theor. Phys. **33**, 423 (1965).

[140] R. Skomski, R. D. Kirby, and D. J. Sellmyer, J. Appl. Phys. **85**, 5069 (1999).

[141] W. F. Brown, J. Appl. Phys. **30**, 625 (1959).

[142] S. V. Vonsovskii, "Ferromagnetic Resonance," Pergamon Press, Oxford 1966.

[143] S. V. Vonsovskii, "Magnetism," John Wiley, New York 1974.

[144] Multidimensional relations are obtained as straightforward vector generalization in spin space, $s \rightarrow \underline{s}$ [5].

[145] H. A. Kramers, Physica **7**, 284 (1940).

[146] P. Hänggi, P. Talkner, and M. Borkovec, Rev. Mod. Phys. **62**, 251 (1990).

[147] F. Bloch, Z. Phys. **61**, 206 (1930).

[148] F. J. Dyson, Phys. Rev. **102**, 1217 (1956).

[149] J. R. Eshbach and R. W. Damon, Phys. Rev. **118**, 1208 (1960).

[150] J. Shen, R. Skomski, M. Klaua, H. Jenniches, S. S. Manoharan, and J. Kirschner, Phys. Rev. B **56**, 2340 (1997).

[151] R. Arias, and D. L. Mills, Phys. Rev. B **63**, 134439 (2001).

[152] J. Jorzick, S. O. Demokritov, B. Hillebrands, M. Bailleul, C. Fermon, K. Y. Guslienko, A. N. Slavin, D. V. Berkov, and N. L. Gorn, Phys. Rev. Lett. **88**, 047204 (2002).

[153] M. I. Chipara, R. Skomski, and D. J. Sellmyer, J. Magn. Magn. Mater. **249**, 246 (2002).

[154] Z. K. Wang, M. H. Kuok, S. C. Ng, D. J. Lockwood, M. G. Cottam, K. Nielsch, R. B. Wehrspohn, and U. Gösele, Phys. Rev. Lett. **89**, 027201 (2002).

[155] K. Y. Guslienko, B. A. Ivanov, V. Novosad, Y. Otani, H. Shima, and K. Fukamichi, J. Appl. Phys. **91**, 8037 (2002).

[156] U. Ebels, J.-L. Duvail, P. E. Wigen, L. Piraux, L. D. Buda, and K. Ounadjela, Phys. Rev. B **64**, 144421 (2001).

[157] P. W. Anderson, Phys. Rev. B **109**, 1492 (1958).

[158] H. Zeng, R. Skomski, L. Menon, Y. Liu, S. Bandyopadhyay, and D. J. Sellmyer Phys. Rev. B **65**, 134426 (2002).

[159] D. J. Sellmyer, M. Yu, R. A. Thomas, Y. Liu, and R. D. Kirby, Phys. Low-Dim. Struct. **1-2**, 155 (1998).

[160] C. P. Bean and J. D. Livingston, J. Appl. Phys. **30**, 120S (1959).

[161] E. P. Wohlfarth, J. Phys. F: Met. Phys. **14**, L155 (1984).

[162] S. W. Charles, in: "Studies of Magnetic Properties of Fine Particles and their Relevance to Materials Science," Eds.: J. L. Dormann and D. Fiorani, Elsevier, Amsterdam 1992, p. 267.

[163] S. F. Edwards and P. W. Anderson, J. Phys. F, **5**, 965 (1975).

[164] The magnetization dynamics of ferrofluids is characterized by the distinction between Brownian and Néel relaxations. Brownian relaxation refers to the mechanical rotation of the particles in a magnetic field, whereas Néel relaxation involves jumps over magnetic energy barriers; the latter dominates in small nanoparticles.

[165] L. Néel, J. de Phys. Rad. **12**, 339 (1951).

[166] P. Gaunt, Phil. Mag. B **48**, 261 (1983).

[167] P. Gaunt, J. Appl. Phys. **59**, 4129 (1986).

[168] R. Skomski and V. Christoph, phys. stat. sol. (b) **156**, K149 (1989).

[169] D. Givord and M. F. Rossignol, in "Rare-earth Iron Permanent Magnets," Ed.: J. M. D. Coey, University Press, Oxford 1996. p. 218.

[170] D. J. Sellmyer, M. Yu, and R. D. Kirby, "Nanostructured Mater," **12**, 1021 (1999).

[171] D. Givord, A. Lienard, P. Tenaud, and T. Viadieu, J. Magn. Magn. Mater. **67**, L281 (1987).

[172] D. Givord, Q. Lu, M. F. Rossignol, P. Tenaud, and T. Viadieu, J. Magn. Magn. Mater. **83**, 183 (1990).

[173] M. P. Sharrock, J. Appl. Phys. **76**, 6413 (1994).

[174] L. Néel, J. de Phys. Rad. **11**, 49 (1950).

[175] R. H. Victora, Phys. Rev. Lett. **63**, 457 (1989); 65, 1171 (1990).

[176] D. J. Sellmyer and R. Skomski, Scripta Materialia **47**, 531 (2002).

[177] J. Moritz, B. Dieny, J. P. Nozieres, Y. Pennec, J. Camarero, and S. Pizzini, Phys. Rev. B **71**, 100402R (2005).

[178] J. D. Livingston and C. P. Bean, J. Appl. Phys. **32**, 1964 (1961).

[179] E. F. Kneller and F. E. Luborsky, J. Appl. Phys. **34**, 656 (1959).

[180] R. Skomski and D. J. Sellmyer, J. Appl. Phys. **89**, 7263 (2001).

[181] J. P. Liu, R. Skomski, Y. Liu, and D. J. Sellmyer, J. Appl. Phys. **87**, 6740 (2000).

[182] F. Preisach, Z. Phys. **94**, 277 (1935).

[183] G. Bertotti and V. Basso, J. Appl. Phys. **73**, 5827 (1993).

[184] P. Wohlfarth, J. Appl. Phys. **29**, 595 (1958).

[185] D. Henkel, Phys. Stat. Sol. **7**, 919 (1964).

[186] X.-D. Che and N. H. Bertram, J. Magn. Magn. Mater. **116**, 121 (1992).

[187] V. Basso, M. LoBue, and G. Bertotti, J. Appl. Phys. **75**, 5677 (1994).

[188] R. J. Veitch, IEEE Trans. Magn. **26**, 1876 (1990).

[189] G. Herzer, Scripta Metal. **33**, 1741 (1995).

[190] H. Fukunaga and H. Inoue, Jpn. J. Appl. Phys. **31**, 1347 (1992).

[191] J. J. Versluijs, M. A. Bari, and J. M. D. Coey, Phys. Rev. Lett. **87**, 026601 (2001).

[192] E. Goto, N. Hayashi, T. Miyashita, and K. Nakagawa, J. Appl. Phys. **36**, 2951 (1965).

[193] Y. Imry and S.-K. Ma, Phys. Rev. Lett. **35**, 1399 (1975).

[194] R. Harris, M. Plischke, and M. J. Zuckermann, Phys. Rev. Lett. **31**, 160 (1973).

[195] E. M. Chudnovsky, W. M. Saslow, and R. A. Serota, Phys. Rev. B **33**, 251 (1986).

[196] D. J. Sellmyer, M. J. O'Shea, in: "Recent Progress in Random Magnets," Ed. D. H. Ryan, World Scientific, Singapore 1992, p. 71.

[197] G. Herzer, J. Magn. Magn. Mater. **112**, 258 (1992).

[198] C. H. Bennet and D. P. DiVincenzo, Nature (London) **404**, 247 (2000).

[199] A. Ekert and R Josza, Rev. Mod. Phys. **68**, 733 (1996).

[200] L. K. Grover, Phys. Rev. Lett. **79**, 325 (1997).

[201] G. Lagmago Kamta and A. F. Starace, Phys. Rev. Lett. **88**, 107901 (2002)

[202] F. Meier, J. Levy, and D. Loss, Phys. Rev. Lett. **90**, 047901 (2003).

[203] J. Tejada, E. M. Chunovsky, E. del Barco, J. M. Hernandez, and T. P. Spiller, Nanotechnology **12**, 181 (2001).

[204] R. Skomski, A. Y. Istomin, A. F. Starace, and D. J. Sellmyer, Phys. Rev. A **70**, 062307 (2004).

[205] R. Skomski, A. Kashyap, Y. Qiang, and D. J. Sellmyer, J. Appl. Phys. **93**, 6477 (2003).

[206] S. Hill and W. K. Wootters, Phys. Rev. Lett. **78**, 5022 (1997).

[207] R. Skomski, A. Y. Istomin, J. Zhou, A. F. Starace, and D. J. Sellmyer, J. Appl. Phys. **97**, 10R511 (2005).

[208] M. S. S. Brooks and B. Johansson, in: "Handbook of Magnetic Materials," Vol. 7, Ed.: K. H. J. Buschow, Elsevier, Amsterdam 1993, p. 139.